NASA/CR-2004-212650

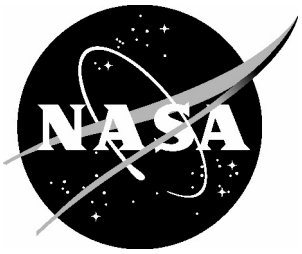

Validation of Design and Analysis Techniques of Tailored Composite Structures

Dulnath D. Wijayratne
The George Washington University
Joint Institute for Advancement of Flight Sciences
Langley Research Center, Hampton, Virginia

December 2004

The NASA STI Program Office . . . in Profile

Since its founding, NASA has been dedicated to the advancement of aeronautics and space science. The NASA Scientific and Technical Information (STI) Program Office plays a key part in helping NASA maintain this important role.

The NASA STI Program Office is operated by Langley Research Center, the lead center for NASA's scientific and technical information. The NASA STI Program Office provides access to the NASA STI Database, the largest collection of aeronautical and space science STI in the world. The Program Office is also NASA's institutional mechanism for disseminating the results of its research and development activities. These results are published by NASA in the NASA STI Report Series, which includes the following report types:

- TECHNICAL PUBLICATION. Reports of completed research or a major significant phase of research that present the results of NASA programs and include extensive data or theoretical analysis. Includes compilations of significant scientific and technical data and information deemed to be of continuing reference value. NASA counterpart of peer-reviewed formal professional papers, but having less stringent limitations on manuscript length and extent of graphic presentations.

- TECHNICAL MEMORANDUM. Scientific and technical findings that are preliminary or of specialized interest, e.g., quick release reports, working papers, and bibliographies that contain minimal annotation. Does not contain extensive analysis.

- CONTRACTOR REPORT. Scientific and technical findings by NASA-sponsored contractors and grantees.

- CONFERENCE PUBLICATION. Collected papers from scientific and technical conferences, symposia, seminars, or other meetings sponsored or co-sponsored by NASA.

- SPECIAL PUBLICATION. Scientific, technical, or historical information from NASA programs, projects, and missions, often concerned with subjects having substantial public interest.

- TECHNICAL TRANSLATION. English-language translations of foreign scientific and technical material pertinent to NASA's mission.

Specialized services that complement the STI Program Office's diverse offerings include creating custom thesauri, building customized databases, organizing and publishing research results ... even providing videos.

For more information about the NASA STI Program Office, see the following:

- Access the NASA STI Program Home Page at ***http://www.sti.nasa.gov***

- E-mail your question via the Internet to help@sti.nasa.gov

- Fax your question to the NASA STI Help Desk at (301) 621-0134

- Phone the NASA STI Help Desk at (301) 621-0390

- Write to:
  NASA STI Help Desk
  NASA Center for AeroSpace Information
  7121 Standard Drive
  Hanover, MD 21076-1320

NASA/CR-2004-212650

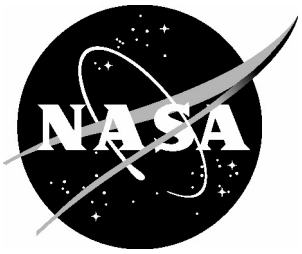

Validation of Design and Analysis Techniques of Tailored Composite Structures

Dulnath D. Wijayratne
The George Washington University
Joint Institute for Advancement of Flight Sciences
Langley Research Center, Hampton, Virginia

National Aeronautics and
Space Administration

Langley Research Center
Hampton, Virginia 23681-2199

Prepared for Langley Research Center
under Cooperative Agreement NCC1-03008

December 2004

Acknowledgments

The author would like to thank the following individuals for making this research possible:

- Dawn Jegley from NASA Langley Research Center for passing on her knowledge of structures and experimentation.
- Dr. Paul Cooper of The George Washington University for his guidance and advice.
- Dr. Damodar Ambur of the Mechanics and Durability Branch at NASA Langley Research Center for providing the opportunity to perform my research.
- Bert Cano and Brian Grimsley for the fabrication of the composite panels.
- Louis Simmons of the Advanced Prototype Development Branch at NASA Langley for all his time and effort.
- Jeff Gragg, Brian Cheshire, George Cowely, Theresa Oneil, and Ann Cole for their assistance in the laboratory.

Table of Contents

Abstract

Aeroelasticity is the relationship between the elasticity of an aircraft structure and its aerodynamics. This relationship can cause instabilities such as flutter in a wing. Engineers have long studied aeroelasticity to ensure such instabilities do not become a problem within normal operating conditions. In recent decades structural tailoring has been used to take advantage of aeroelasticity. It is possible to tailor an aircraft structure to respond favorably to multiple different flight regimes such as takeoff, landing, cruise, 2-g pull up, etc. Structures can be designed so that these responses provide an aerodynamic advantage.

This research investigates the ability to design and analyze tailored structures made from filamentary composites. Specifically the accuracy of tailored composite analysis must be verified if this design technique is to become feasible. To pursue this idea, a validation experiment has been performed on a small-scale filamentary composite wing box. The box is tailored such that its cover panels induce a global bend-twist coupling under an applied load. Two types of analysis were chosen for the experiment. The first is a closed form analysis based on a theoretical model of a single cell tailored box beam and the second is a finite element analysis. The predicted results are compared with the measured data to validate the analyses.

The comparison of results show that the finite element analysis is capable of predicting displacements and strains to within 10% on the small-scale structure. The closed form code is consistently able to predict the wing box bending to 25% of the measured value. This error is expected due to simplifying assumptions in the closed form analysis. Differences between the closed form code representation and the wing box specimen caused large errors in the twist prediction. The closed form analysis prediction of twist has not been validated from this test

List of Figures

Nomenclature

Symbol	Units	Description
A	lb/in.	Laminate extension stiffness matrix
C_{44}, C_{45}, C_{55}	lb-in.^{2}	Global torsion, coupling, and bending stiffness
C_A	inches	Aerodynamic chord, or width
C_S	inches	Structural chord, or box width
D	lb-in.	Laminate bend stiffness matrix
E_{11}	Psi	Longitudinal modulus of elasticity
E_{22}	Psi	Transverse modulus of elasticity
H, L	inches	Height and length of structural wing box
M_x,M_y	lb-in.	Moments about x and y axis respectively
P	lb	Load
S	Psi	Shear strength
w	inches	Vertical displacement (z-axis)
$w_{,xx}$	inches	Bending curvature
X	Psi	Longitudinal strength
Y	Psi	Transverse strength

Symbol	Units	Description
β	-	Bend twist coupling parameter
ϕ	radians	Box twist
$\phi_{,x}$	radians	Rate of twist
$\mu\varepsilon$	-	Microstrain or 10^{-6} inches/inch
ν_{12}	-	Poisson's ratio
θ	degrees	off-axis angle of angle ply

Acronym	Description
AR	Angle Ply Rotation
BTE	Bottom Trailing Edge
BLE	Bottom Leading Edge
DCDT	Direct Current Displacement Transducer
CFC	Closed Form Code
LR	Laminate Rotation

Chapter 1 : Introduction

In the aerodynamics discipline engineers have always understood that the optimal shape of a wing is dependent upon the particular stage of flight. Engineers use devices such as slats and flaps to modify the camber and angle of attack of a wing in flight. The compromise of adding such devices is increased weight and complexity. With structural tailoring using filamentary composites, it may be possible to design a wing to provide deformations under flight loads that result in an increase in aerodynamic performance.

An example of aeroelastic tailoring is the wing design of the X-29 technology demonstrator (Figure 1-1). The X-29 has swept forward wings, which is a configuration that encounters low-speed divergence. This problem was solved by tailoring the skin material to induce a wing bend-twist coupling that counters the divergence[1]. In the sweptback configuration, an aircraft's wings do not encounter the low speed elastic divergence that the X-29 must withstand. However, the tailoring may instead be used for a performance enhancement.

Figure 1-1: X-29 Technology Demonstrator (Photo by NASA)

Previous research on tailored structures allowed the development of analytical tools to quantify their behavior. However little experimentation has been performed to validate the analyses. Before these tools can be used to design structure, they must be validated with actual specimens.

1.1 Objectives

This research focuses on the design, analysis, and testing of a small-scale wing box (Figure 1-2) for the purposes of design and analysis validation. The wing box represents the structural component of a composite wing. The objectives of the research are as follows:

1. Design a small-scale tailored wing box that can measurably demonstrate box bend-twist coupling. Conduct an experiment to measure the behavior of the wing box specimen
2. Analyze the box to predict its response under load using a closed form code (CFC) and a finite element analysis (FEA). Compare these predicted values to the measured values to help validate the analyses.

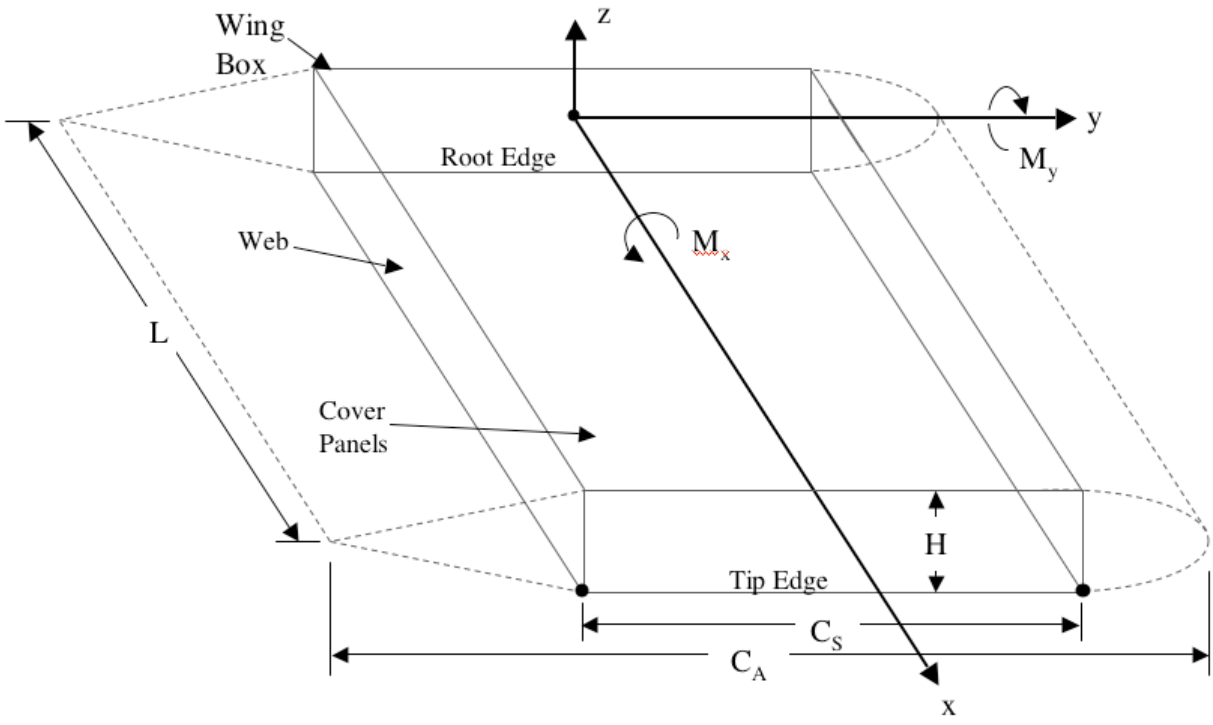

Figure 1-2: Starboard Structural Wing Box

1.2 Review of Literature

Research regarding structural tailoring can be found as far back as the 1940's. Engineers proposed orienting wood fibers in propellers to provide a favorable elastic response. In the early 1980's a body of work was completed regarding the use of aeroelastic tailoring to solve the low speed divergence problem of swept forward wings. A paper written by Sherrer, Hertz, and Shirk describes a wind tunnel demonstration of tailoring in a swept forward wing[2]. Shirk also co-wrote a paper validating aeroelastically tailored design methods for selected wing configurations[3]. Also in the 1980's, Valisetty and Rehfield developed a theoretical beam model for the use in composite rotor blades[4]. This model considers a single cell box beam with tailored cover panels

that induce a bend-twist coupling in the beam. Later Rehfield co-wrote a paper with Hodges and Nixon that correlated the single cell beam model with an MSC/NASTRAN finite element model[5]. A NASA contractor report by Rehfield, Chang, and Zischka describe methods of chord-wise aeroelastic tailoring[6].

More recently a paper written by Rehfield and Cheung extends the tailored box model analysis by developing rate-of-twist and bending-curvature formulas[7]. These are the governing equations used to create the closed form code in this research. Rehfield and Cheung also use the simple tailored box model in an optimization code. Minimum weight stacking sequences are found as a function of the ply rotation angle while constrained by a maximum axial strain in the fiber direction.

Chapter 2 : Design and Fabrication

To validate the analysis methods, they must be compared to the response of an actual test specimen. A small-scale tailored wing box was designed and fabricated from filamentary composites at NASA Langley Research Center for this purpose. Using a structural tailoring technique, the wing box specimen was designed to exhibit bend-twist coupling under load. The design and fabrication process is discussed in this chapter.

2.1 Methods of Filamentary Composite Tailoring

Structural tailoring involves the implementation of directional stiffness to control the deformations caused by external forces[1]. Filamentary composite materials can be used to create these stiffnesses. Fibers can be oriented in any direction to provide the required behavior. Two strategies for tailoring of composites described in reference 7 are the Laminate Rotation (LR) method and the Angle ply Rotation (AR) method.

2.1.1 Laminate Rotation

In this strategy a stacking sequence is selected that contains a combination of axial, transverse and angle plies. In most cases a balanced laminate ($-\theta$ to match each $+\theta$) is chosen to avoid difficulties during fabrication[7]. The resulting balanced panel has orthotropic properties. The entire laminate is then rotated such that the principal material axes are not aligned with the natural body axes of the structure, as shown in Figure 2-1, producing an unsymetric response when loaded[8].

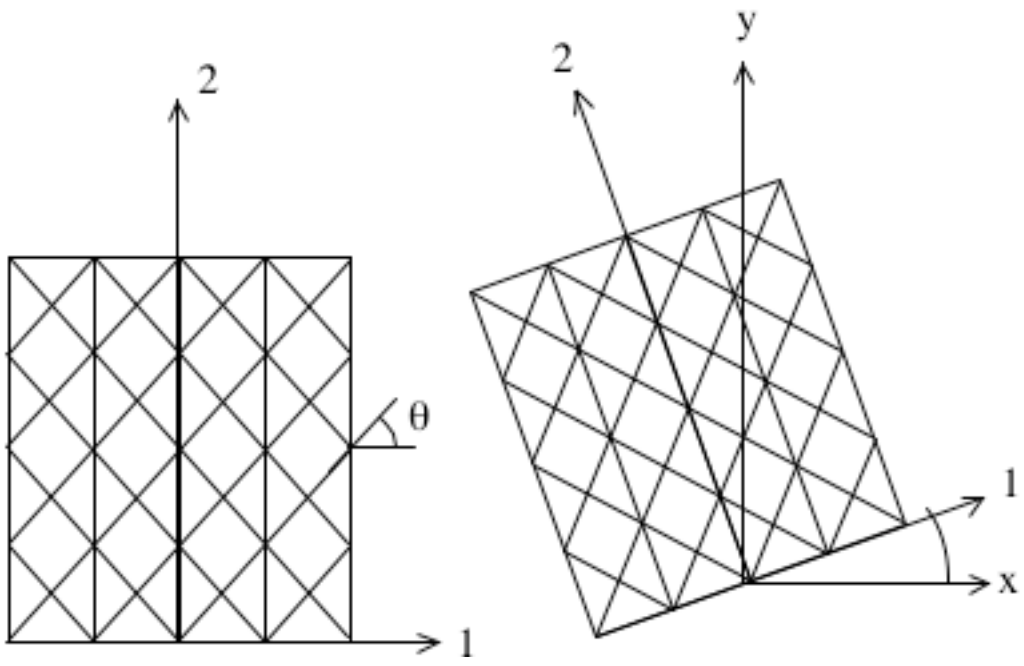

Figure 2-1: Laminate Rotation Strategy

This method was utilized in the fabrication of the X-29 wing (Figure 1-1). Normally the aerodynamic divergence of a swept forward wing would lead to wing failure. The LR skin was applied to the wing such that it exhibits bend-twist coupling. This coupling counters the divergent twisting caused by the loading on a forward swept wing[2].

2.1.2 Angle Ply Rotation

The second approach involves designing a stacking sequence that is optimized to produce the desired behavior. Unbalanced angle plies (i.e., no -θ plies to counter the +θ plies) are added to 0° and 90° plies to provide the directional stiffnesses as shown in Figure 2-2. This method has the potential to be more efficient than the LR strategy since all plies contribute toward the desired behavior[7]. The magnitude of the shear-extension and bend-twist coupling terms, which

are necessary for tailoring, depend on the stacking sequence and number of plies. As the number of plies increases the coupling terms tend to vanish.

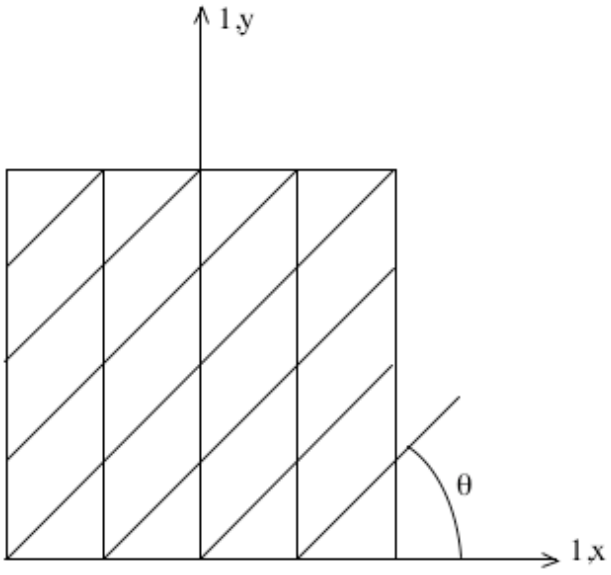

Figure 2-2: Angle Ply Rotation Strategy

Neither strategy requires stacking sequences that are unsymmetric about the mid-plane. A symmetric arrangement is generally desirable from a manufacturing aspect to avoid warping caused by thermally induced loads during the curing process on a laminate with bend-extension coupling. The shear-extension coupling can also affect the laminate when cooled but will not directly cause out-of-plane deformations[8].

2.1.3 Box Bend-Twist Coupling

The specific deformation of interest in this research is the box bend-twist coupling that can be induced under an applied load. The simple tailored box model as described in reference 2 considers only the cover panels to be the load-bearing component. Therefore box tailoring occurs

through these panels. To understand the global box bend-twist coupling mechanism, the panel behavior must be examined.

A laminate's behavior can be described by its stiffness matrices found in the force and moment equations (Eq. 2-1 and 2-2).

$$\begin{bmatrix} N_x \\ N_y \\ N_{xy} \end{bmatrix} = \begin{bmatrix} A_{11} & A_{12} & A_{16} \\ A_{12} & A_{22} & A_{26} \\ A_{16} & A_{26} & A_{66} \end{bmatrix} \cdot \begin{bmatrix} \varepsilon_x^{\circ} \\ \varepsilon_y^{\circ} \\ \gamma_{xy}^{\circ} \end{bmatrix} + \begin{bmatrix} B_{11} & B_{12} & B_{16} \\ B_{12} & B_{22} & B_{26} \\ B_{16} & B_{26} & B_{66} \end{bmatrix} \cdot \begin{bmatrix} \kappa_x \\ \kappa_y \\ \kappa_{xy} \end{bmatrix} \qquad \text{Eq. 2-1}$$

$$\begin{bmatrix} M_x \\ M_y \\ M_{xy} \end{bmatrix} = \begin{bmatrix} B_{11} & B_{12} & B_{16} \\ B_{12} & B_{22} & B_{26} \\ B_{16} & B_{26} & B_{66} \end{bmatrix} \cdot \begin{bmatrix} \varepsilon_x^{\circ} \\ \varepsilon_y^{\circ} \\ \gamma_{xy}^{\circ} \end{bmatrix} + \begin{bmatrix} D_{11} & D_{12} & D_{16} \\ D_{12} & D_{22} & D_{26} \\ D_{16} & D_{26} & D_{66} \end{bmatrix} \cdot \begin{bmatrix} \kappa_x \\ \kappa_y \\ \kappa_{xy} \end{bmatrix} \qquad \text{Eq. 2-2}$$

The A, B, and D matrices represent the extension, bending-extension coupling, and the bending stiffness, respectively, of a laminate. Since all laminates fabricated for this experiment are symmetric about the mid-plane, the bending-extension (B) matrix disappears. In a generally orthotropic laminate, the A and D matrices are fully populated. The appearance of the A_{16} and A_{26} terms indicate an extension-shear coupling while the D_{16} and D_{26} terms indicate bend-twist coupling.

Both sets of coupling terms influence the deformation of a panel. However in the tailored box model, the author of reference 4 makes the assumption that no panel bending occurs, only extension. Therefore only the extension-shear coupling term is considered to contribute to box deformation, thus the D matrix is ignored in the calculations. When the wing box is in bending, one cover panel will be in tension and the other in compression. These forces cause opposite extension in each cover panel and, through the coupling, opposite shear deformation (Figure 2-3). These deformations induce a torque which results in box twist as shown in Figure 2-4.

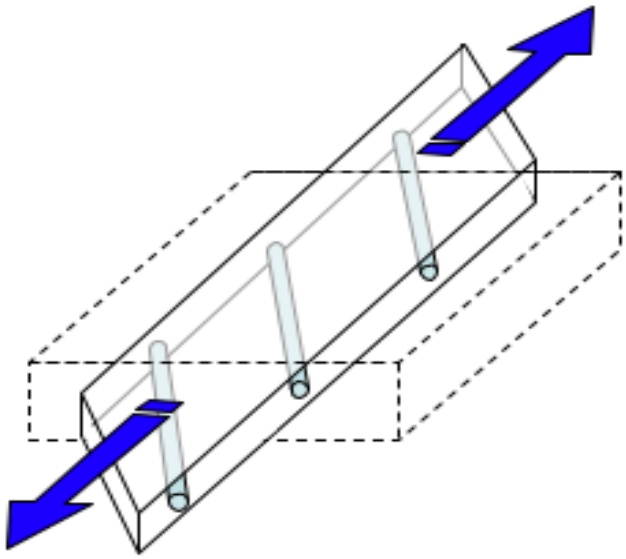

Figure 2-3: Extension-Shear Coupling in Generally Orthotropic Laminates

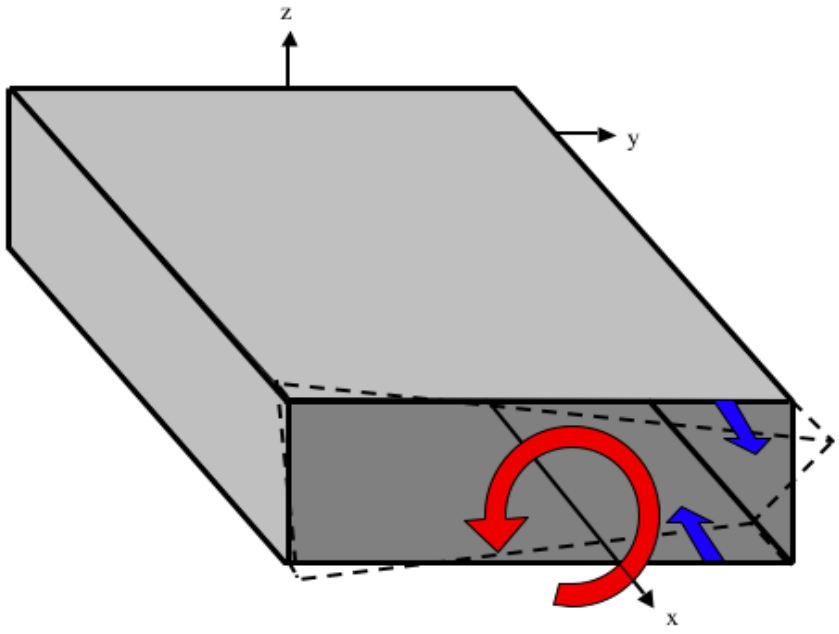

Figure 2-4: Box Bend-Twist Coupling caused by Laminate Shear-Extension Coupling

2.2 Wing Box Specimen Design

The design goal set for the box is to demonstrate the bend-twist coupling phenomenon. Therefore the tailored cover panels were designed to maximize this effect. For the same reason, the response (displacements and strains) must be measurable. The Direct Current Displacement Transducers (DCDT's) used in this test require a displacement of at least 0.01 inches to confidently disregard experimental error due to noise, imperfect boundary conditions, etc.

The wing box consists of three main parts; the cover panels, web panels, and angle brackets. The cover panels are the primary load bearing pieces of the structure and are the tailored components. The webs are loaded primarily in shear and were designed as symmetric laminates with orthotropic behavior such that they should not affect the bend-twist coupling. Similarly the brackets are designed to minimize the impact on the behavior of the tailored box. The lower two brackets are molded from the same composite as the box while the upper two brackets are made of aluminum. All brackets are bonded to the wing box to hold the assembly together.

The maximum dimensions of the wing box were limited by the tooling available to fabricate composite panels. The largest panel that could be created was approximately 33 inches by 20 inches. Preliminary studies completed with the CFC and FEA model indicated that a structure of this relative size would exhibit very small deflections. Therefore the length was set to the maximum manufacturable length of 33 inches to maximize the end displacement. One inch of the span at the wing root would be potted to represent the clamped boundary conditions, leaving a wing box span of 32 unsupported inches. The cover panels are 14 inches wide with 1

inch on either side for fixturing, leaving a 12-inch chord for the box. The box height is 2.27 inches. The wing box specimen is illustrated in Figure 2-5.

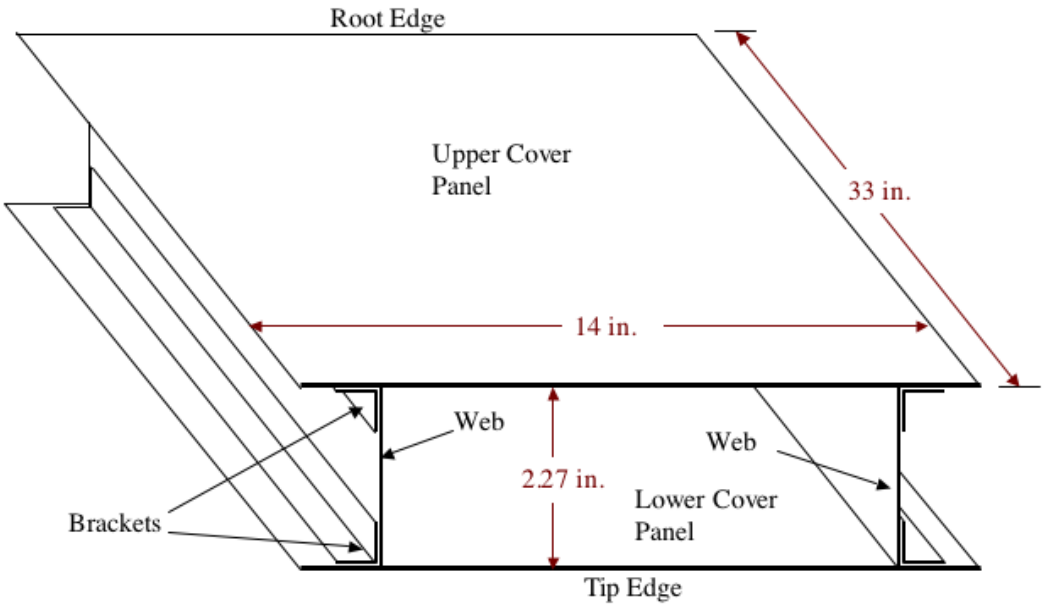

Figure 2-5: Wing Box Specimen Dimensions

With the box dimensions in place, the stacking sequences of the cover panels are designed to maximize bend-twist coupling. To determine the properties of each panel, the membrane stiffness (A matrix) of each composite panel is found.

$$A_{ij} = \sum_{k=1}^{N} \overline{Q_{ij}^{(k)}} h_k \quad (i,j = 1,2,6) \qquad \text{Eq. 2-3}$$

N refers to the total number of plies, h_k is the thickness of ply k, and $Q_{ij}^{(k)}$ is the reduced stiffness matrix for ply k. The A matrix can be used to find the uniaxial wall plane stress stiffnesses[6]:

$$K_{11} = A_{11} - (A_{12})^2 / A_{22} \quad \text{(Extension)} \qquad \text{Eq. 2-4}$$

$$K_{12} = A_{16} - (A_{12}A_{26}) / A_{22} \quad \text{(Shear)} \qquad \text{Eq. 2-5}$$

$$K_{22} = A_{66} - (A_{26})^2 / A_{22} \quad \text{(Coupling)} \qquad \text{Eq. 2-6}$$

These stress stiffnesses are then used to find the global box stiffness[7]:

$$C_{44} = \frac{Cs^2H^2}{(Cs+H)^2}\left[(K_{22}^{u} + K_{22}^{l})Cs + (A_{66}^{TE} + A_{66}^{LE})H\right] \quad \text{Eq. 2-7}$$

$$C_{45} = \frac{Cs^2H^2}{2(Cs+H)}\left[K_{12}^{u} + K_{12}^{l}\right] \quad \text{Eq. 2-8}$$

$$C_{55} = \frac{CsH^2}{4}\left[K_{11}^{u} + K_{11}^{l}\right] \quad \text{Eq. 2-9}$$

C_{44}, C_{45}, and C_{55} are the box torsion, coupling, and bending stiffnesses respectively. In reference 7, the value β^2 is defined as a bend-twist coupling parameter.

$$\beta^2 = \frac{(C_{45})^2}{C_{44} \cdot C_{55}} \quad \text{Eq. 2-10}$$

Higher values of β^2 indicate a greater coupling. A parametric study conducted with the optimization code in reference 7 is used to determine the effect of angle plies on β^2. The bend-twist coupling parameter peaks in magnitude between angle plies of 30° to 32° as shown in Figure 2-6.

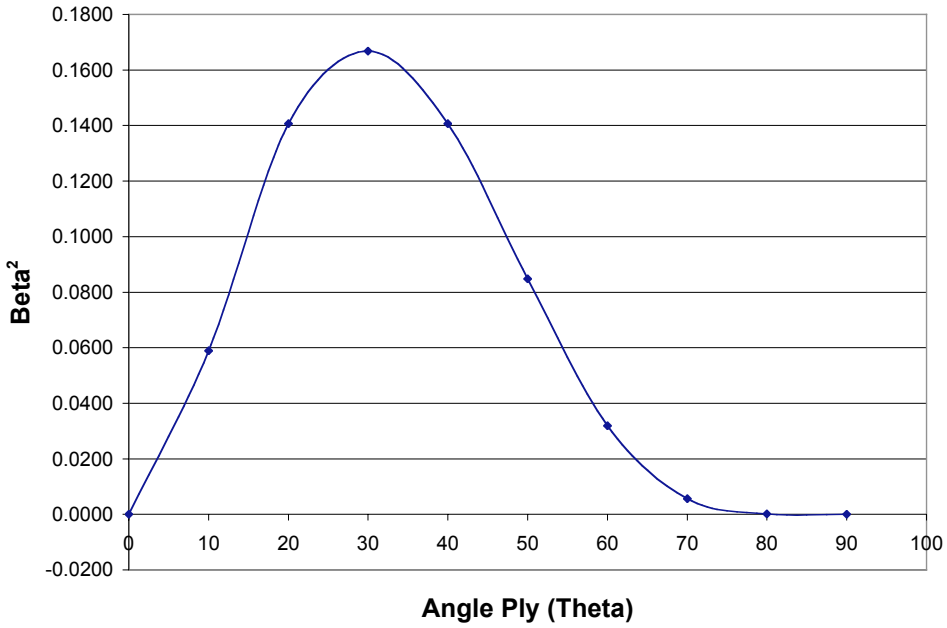

Figure 2-6: Bend-Twist Coupling Parameter vs. Angle Ply $[0/\theta/90]_s$

Several stacking sequences with angle plies near this peak are evaluated in the finite element model to establish a design that would maximize box bending and twisting. The stacking sequence of the final upper cover panel design is $[35/90/35/(45/90)_2]_S$. The lower cover panel is $[-35/90/-35/(-45/90)_2]_S$, which is a mirror image of the upper panel. With this orientation, the K_{12} wall plane stress stiffness terms are equal in magnitude but opposite in sign, effectively doubling the C45 coupling term[6].

$$C_{45} = \frac{C^2 H^2}{2(C+H)}(K_{12}^u - K_{12}^l) = \frac{C^2 H^2}{(C+H)} K_{12} \qquad \text{Eq. 2-11}$$

Both the webs and lower brackets had ply orientations of $[\pm 45]_S$ so that they should not effect the coupling stiffness. The top brackets were cut from 1/16th inch angle stock of Aluminum 7075-T6.

2.3 Panel and Box Fabrication

Facilities operated by the Advanced Materials and Processing Branch at the NASA Langley Research Center were used to manufacture all of the composite panels. The composite fabrication process used is called Vacuum Assisted Resin Transfer Molding (VARTM). This technique does not require an autoclave, which makes it more flexible in terms of panel size and reduces cost. VARTM was chosen as the fabrication process because it has been successful in creating panels with unbalanced stacking sequence without warping as required by the AR strategy.

Fabrication begins with the stacking of unidirectional fabric at different angles to create the desired stacking sequence. The fabric consisted of Magnamite IM7 high performance fibers in a 6K-filament count. The fabric is then enclosed in a conformable bag to which a vacuum is drawn. VR56-19 VARTM resin flows into the bag and infiltrates the fibers as see in Figure 2-7. Once fully impregnated, the part is placed in an oven to cure. The cure cycle consists of a ramp up from room temperature to 67°C at 1.1°C/minute and hold for 2.75 hours, followed by a ramp at 1.4°C/minute to 123°C and hold for another 2.75 hours. The part is then cooled at 1.0°C/minute to room temperature, released from the mold and subjected to a freestanding post cure for six hours at 177°C[9].

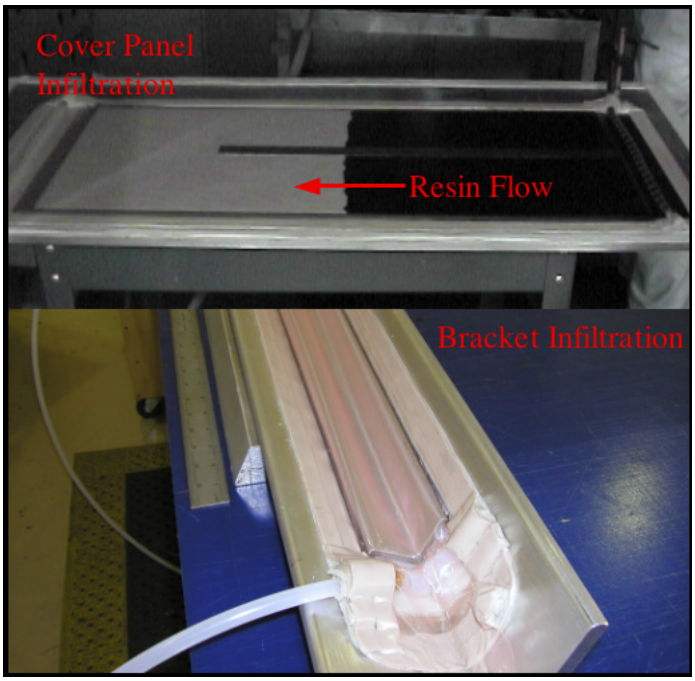

Figure 2-7: Resin Infiltration

A total of five composite panels were fabricated. Two were created for the cover panels with the tailored stacking sequence and designated panel C1 and C2. Another two unidirectional panels, labeled TS-1 and TS-2, were created for a set of material property tests. The fifth was fabricated with the $[\pm 45]_s$ ply stacking sequence for the webs.

The quality of each panel was verified using ultrasonic C-scans, a form of non-destructive evaluation, to reveal any imperfections in the composite matrix. Figures 2-8 and 2-9 show the results from the cover panels. A dark uniform color indicates good consistent resin density while lighter spots can indicate imperfections. The scan of panel C1 shows a uniform density throughout its area while panel C2 has a few locations along one side of the panel that is less dense than the rest of the matrix. The largest defects can be found along the topside of the panel (as oriented in figure). Air bubbles or dry spots in which the fibers were not thoroughly

infiltrated by the resin can cause these features. Both conditions are undesirable since they can reduce the local strength of the structure. Fortunately this imperfection does not greatly affect the overall strength of the box for several reasons. Each panel was fabricated slightly larger than necessary so the edges could be trimmed off. Secondly panel C2 was designated as the upper cover and oriented such that the bubbles reside in a lower stress area. Since the loads applied to the box do not put the panel near its ultimate load during the main test, the imperfection was not expected to become an issue. The scan of panel TS-2, shown in Figure 2-10, also revealed significant resin density variation. Scans of C1, TS-1, and the web panel did not reveal any major imperfections.

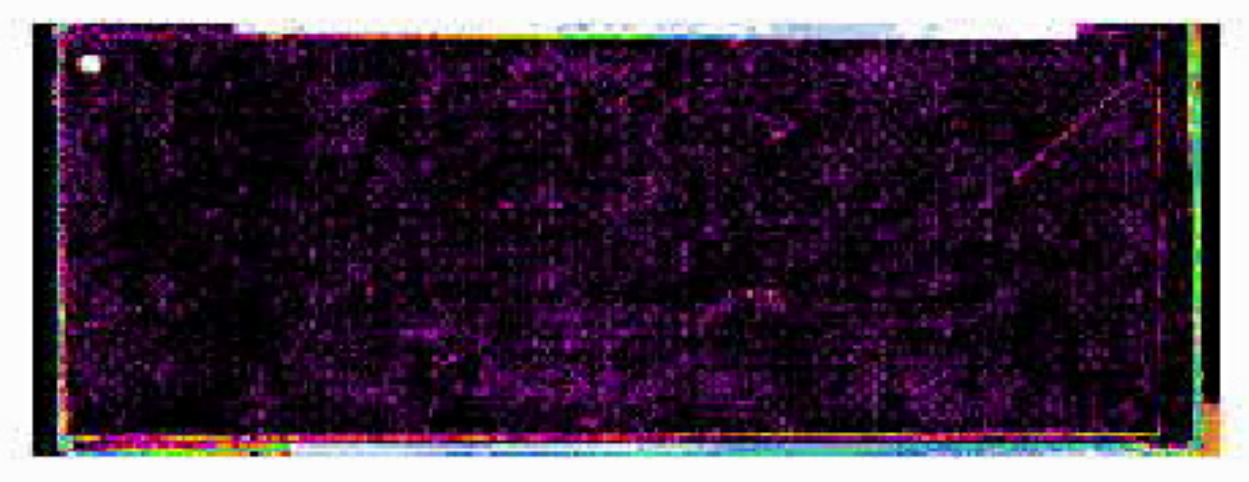

Figure 2-8: C-scan of Panel C1

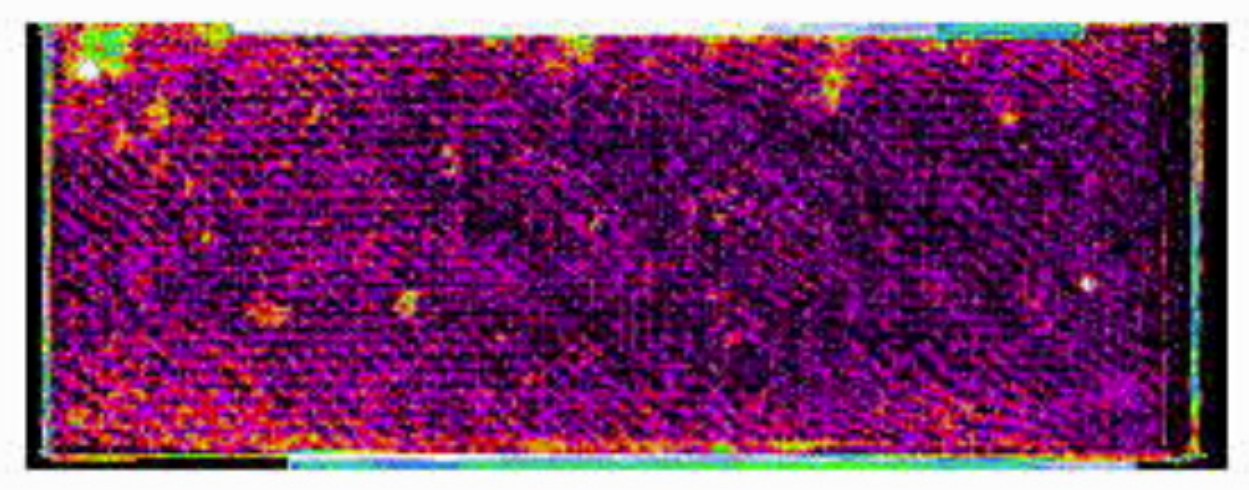

Figure 2-9: C-scan of Panel C2

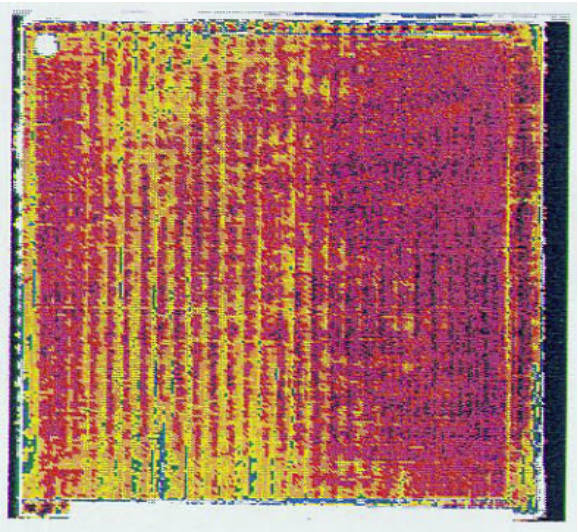

Figure 2-10: C-scan of Panel TS-2

The two cover panels were checked for geometric imperfections. In this case the goal was to quantify the thickness variation throughout the panel's length. The thickness of panel C2 varied by approximately ±0.009 inches and panel C1 varied by ±0.008 inches (Figure 2-11 and 2-12). This variation is nearly 10% of the panel thickness, which may affect the accuracy of the

analysis. An approximate thickness of 0.086 inches was used for both cover panels in the analyses.

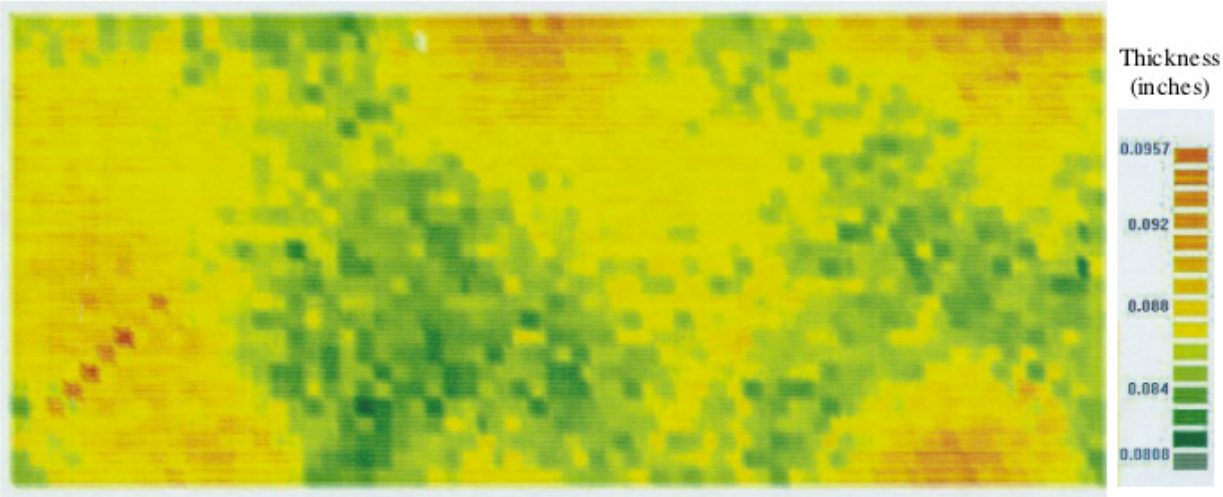

Figure 2-11: Panel C1 Thickness Variation

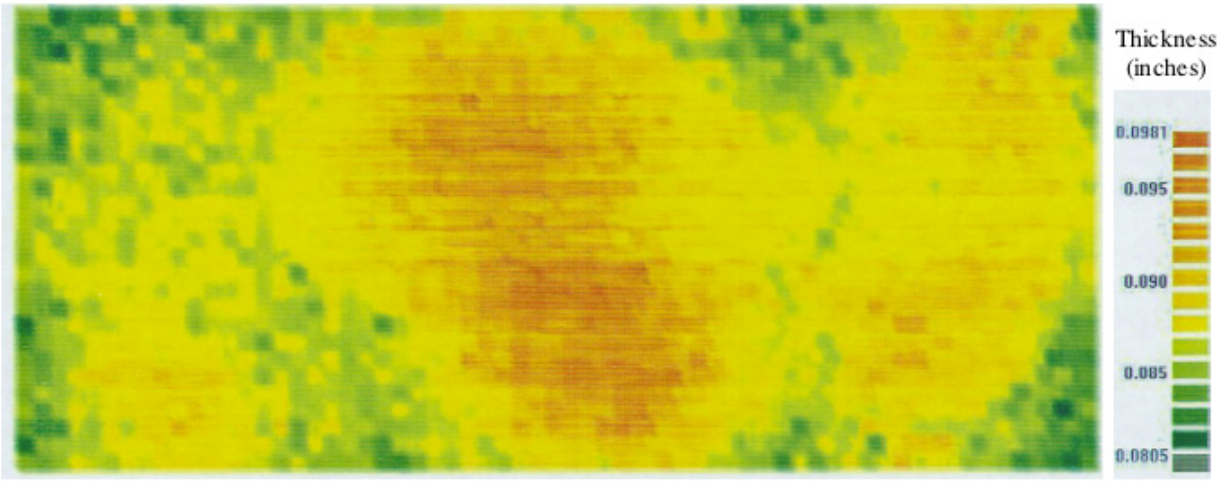

Figure 2-12: Panel C2 Thickness Variation

With all the parts in hand the box panels were assembled together with the brackets using Loctite Hysol 934, a room temperature adhesive. The final fabrication step involved potting 1-

inch of the root end of the box in a resin-aluminum mixture that is cured in an aluminum mold. The root end of the wing box is placed in the mixture while it is curing. When hardened the potting provides a stiff root edge that is represented by clamped boundary conditions in the finite element model. It also distributes boundary loads without causing local failure. The potting frame is clamped to the test wall to complete the clamped conditions.

2.4 Mechanical Property Tests

Since the material used to create the panels is a relatively new fiber and resin system, material characterization was required. Two mechanical property tests were completed for this purpose. These tests were completed in accordance with the American Society for Testing of Materials (ASTM D 3039)[10]. Properties that were obtained from these tests include E_{11}, E_{22}, and ν_{12}.

2.4.1 Specimens

Fifteen specimens were cut from unidirectional panel TS-1 with the fibers in the longitudinal or 0° direction and were labeled TS-1-1 through TS-1-15. Ten specimens were cut from unidirectional panel TS-2 with the fibers transverse, or 90°, from the loading direction. These transverse specimens were labeled TS-2-1 through TS-2-10. Since the C-scan of panel TS-2 revealed some resin variation, the specimens were sampled from different areas of the panel to determine if the resin density affected the results. Each specimen was 0.5 inches wide and 10 inches long. Specimens TS-1-1 through TS-1-8 were instrumented with longitudinal gages and TS-1-9 to TS-1-15 were instrumented with transverse gages. The TS-2 specimens were

instrumented with both longitudinal and transverse gages. All gages were set back-to-back and centered both axially and transversely. To protect the specimens from the test machine grips, fiberglass tabs were bonded to both ends. The specimen specifications are illustrated in Figure 2-13.

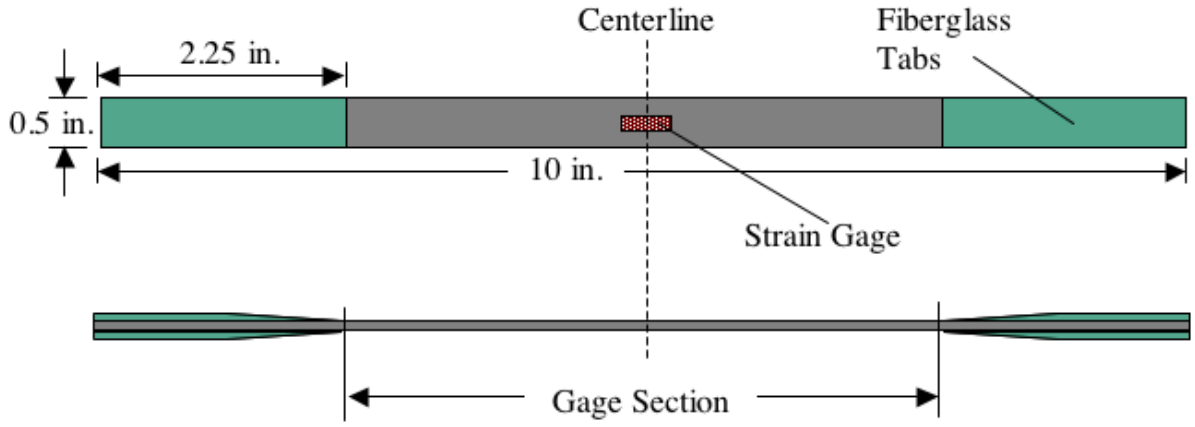

Figure 2-13: Tension Specimen (axial gage shown)

2.4.2 Test Setup and Procedure

Each test was performed on a Material Test Stand (MTS) 50 kip machine. The test stand was operated with an MTS 458.20 controller and the data were acquired with a VISHAY System 5000 scanner. The specimens were gripped in the hydraulic jaws of the test stand. Care was taken to align the longitudinal axis of the specimen with the axis of the test stand. The strain gages, load cell, and displacement sensor were all set to zero prior to test start. Data was sampled from the specimen at a rate of 1 measurement per second for the TS-1 specimens and 2 measurements per second for the TS-2 specimens. The MTS stand loaded the tension specimens

in strain control mode at 0.05 inches/minute until failure. After failure the maximum load and failure location and type were noted.

2.4.3 Property Test Results

Most of the tension specimens failed in the grip region so failure information is not representative of the specimen strength. The elastic modulus E_{11} is calculated from data from specimens TS-1-1 through TS-1-8 using the relationship $E = \Delta\sigma/\Delta\varepsilon$ and is shown in Table 2-1. The stress between 1000 and 3000 με is used for the calculation. The remaining TS-1 specimens provide the relationship between longitudinal strain and transverse strain required to calculate $\nu_{12} = -\Delta\varepsilon_l/\Delta\varepsilon_t$ as shown in Table 4-2. Finally the TS-2 specimens are used to find E_{22} shown in Table 4-3. A range of 500 to 2500 με was used for the calculations. The coefficient of variation for the calculation of E_{22} is only 0.8%. The minor variation in resin density in panel TS-2 did not seem to affect the results of the test. The shear modulus of elasticity was taken from the resin manufacturer's data sheet and was G_{12} = 0.64 msi[14].

Table 2-1: Calculation of Elastic Modulus E_{11}

Specimen	*Strain 1 (Microstrain)*	*Strain 2 (Microstrain)*	*Stress 1 (psi)*	*Stress 2 (psi)*	*Modulus of Elasticity E_{11}(psi)*
TS-1-1	1014	2984	19560	59030	2.00×10^7
TS-1-2	1004	3037	18690	57820	1.93×10^7
TS-1-3	1020	2965	19520	58040	1.98×10^7
TS-1-4	1033	2971	19740	58090	1.98×10^7
TS-1-5	1013	2995	19270	58380	1.97×10^7
TS-1-6	1021	2977	20250	60550	2.06×10^7
TS-1-7	981	2989	20160	62660	2.12×10^7
TS-1-8	977	2998	19600	61370	2.07×10^7
				Average E_{11} =	**2.01×10^7psi**
				Standard Deviation =	**583000 psi**
				Coefficient of Variation =	**2.9%**

Table 2-2: Calculation of Poisson's Ratio

	Strain 1 (Microstrain)	*Strain 2 (Microstrain)*	*$\Delta\varepsilon$*
longitudinal	1000	3000	2000
transverse	-308	-929	-620
			ν_{12} = 0.310

Table 2-3: Calculation of Elastic Modulus E_{22}

Specimen:	*Strain 1 (microstrain)*	*Strain 2 (microstrain)*	*Stress 1 (psi)*	*Stress 2 (psi)*	*Modulus of Elasticity E_{22}(psi)*
TS-2-1	532	2502	782	3685	1.47×10^6
TS-2-2	498	2539	758	3756	1.47×10^6
TS-2-3	532	2538	812	3729	1.45×10^6
TS-2-4	510	2506	758	3670	1.46×10^6
TS-2-5	493	2536	734	3754	1.48×10^6
TS-2-6	496	2512	783	3792	1.49×10^6
TS-2-7	512	2510	798	3768	1.49×10^6
TS-2-8	512	2496	807	3740	1.48×10^6
TS-2-9	511	2502	803	3742	1.48×10^6
TS-2-10	498	2526	759	3734	1.47×10^6
				Average E_{22} =	**1.47×10^6 psi**
				Standard Deviation =	**11100 psi**
				Coefficient of Variation =	**0.8%**

Chapter 3 : Analysis

Engineers benefit from an analytical tool to aid in the design of tailored structures. The finite element technique can provide an accurate analysis of a structure. However creating a finite element model can be time consuming. A closed form analysis provides a fast alternate that may be helpful to a designer. Both of these techniques are applied to the wing box specimen to predict its behavior. The predicted results are compared with the measured values in Chapter 5.

3.1 Closed Form Analysis

The work by Cheung in reference 7 regarding tailored composite box beams provides the mathematical groundwork for the closed form code. The author develops an analytical model of a single cell box beam by using the simplified tailored box model based on the theory of thin walled composite beams by Rehfield[6]. By extending this work, a closed form code (CFC) is written in Matlab to provide twist (ϕ) and deflection (w) of a simplified wing box given geometry, material properties, and loading information.

3.1.1 Derivation

The model is a pair of cover panels that are connected by two web panels. This box represents the load bearing structure of a composite wing (Figure 1-2). Boundary conditions for the model are set to represent an aircraft wing with a clamped root and a free end. The Rate of Twist of the wing and the Bending Curvature are derived in reference 3 and can be found from the following expressions:

$$\phi_{,x} = \frac{1}{C_{44}C_{55}(1-\beta^2)}(C_{55}M_x - C_{45}M_y) \quad \text{Eq. 3-1}$$

$$w_{,xx} = \frac{1}{C_{44}C_{55}(1-\beta^2)}(C_{45}M_x - C_{44}M_y) \quad \text{Eq. 3-2}$$

The terms M_x and M_y are moments about the span-wise axis (x) and chord-wise axis (y), respectively.

A more useful set of equations would provide the actual magnitude of twist and vertical displacement with respect to x, or span. The first, $\phi(x)$, can be obtained by integrating equation 3-1 with respect to x.

$$\phi(x) = \int_0^x \phi_{,\lambda}\, d\lambda = \int_0^x \frac{1}{C_{44}C_{55}(1-\beta^2)}(C_{55}M_x - C_{45}M_y)d\lambda \quad \text{Eq. 3-3}$$

The global stiffness and bend-twist coupling parameters are dependent solely on the material system and box cross-section, which are constant in this experiment. They can therefore be moved outside the integral. Moments M_x and M_y are functions of x and are determined by the distribution of loads. Since the relationship is linear, the contribution to twist from each load can be evaluated separately and then summed to find the total wing twist. In a general form, the twist at point x on a wing box with N loads is expressed as:

$$\phi(x) = \frac{1}{C_{44}C_{55}(1-\beta^2)} \times \left[\sum_{i=1}^{N} \int_0^{u_i} (C_{55}M_{x_i} - C_{45}M_{y_i})d\lambda\right] \quad \text{Eq. 3-4}$$

$$u_i = \begin{cases} d_i & x > d_i \\ x & x < d_i \end{cases}$$

N refers to the number of loads on the wing box and d_i is the span-wise distance of load i from the root. An example of a multiple load scenario is illustrated in Figure 3-1.

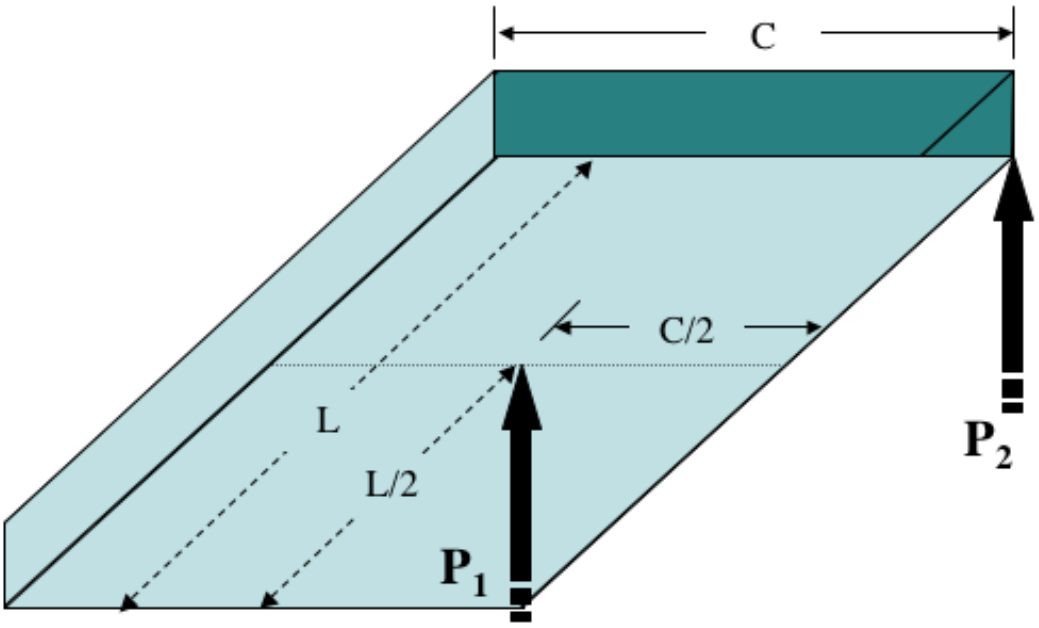

Figure 3-1: Multiple Load Scenario

In this example there are two loads (N=2). The moments about the x-axis are $M_{x_1} = 0$ and $M_{x_2} = Py$. The moments about the y-axis due to the two loads are $M_{y_1} = -P_1(L/2 - x)$ and $M_{y_2} = -P_2(L - x)$. Equation 3-4 would expand to:

$$\phi(x) = \frac{1}{C_{44}C_{55}(1-\beta^2)} \times \left[\int_0^{L/2} (-C_{45}M_{y_1})d\lambda + \int_0^{x} (C_{55}M_{x_2} - C_{45}M_{y_2})d\lambda \right] \qquad \text{Eq. 3-5}$$

For the purpose of this research the wing box specimen is loaded as a cantilever beam, with a single point load along the tip edge. In this load case $M_x = P \cdot y$ and $M_y = -P(L - x)$ throughout the entire span (N=1). The corresponding twist equation is:

$$\phi(x) = \frac{1}{C_{44}C_{55}(1-\beta^2)} \int_0^{x} \left[C_{55}(Py) + C_{45}P(L-\lambda) \right] d\lambda \qquad \text{Eq. 3-6}$$

which upon evaluation becomes a quadratic of x:

$$\phi(x) = \frac{P}{C_{44}C_{55}(1-\beta^2)}\left[(C_{55}y + C_{45}L)x - \frac{1}{2}C_{45}x^2\right] \qquad \text{Eq. 3-7}$$

Similarly, the deflection in the vertical direction can be found to be a cubic of x:

$$w(x) = \frac{P}{C_{44}C_{55}(1-\beta^2)}\left[(C_{45}y + C_{44}L)\frac{x^2}{2} - C_{44}\frac{x^3}{6}\right] \qquad \text{Eq. 3-8}$$

The constants of integration disappear due to the clamped boundary conditions (i.e., $\phi(0)=0$, $dw/dx(0)=0$, and $w(0)=0$). With equations 3-7 and 3-8 the CFC model, illustrated in Figure 3-2, can be used to evaluate a wing box design. The CFC plots ϕ vs. span and w vs. span are shown in figures 3-3 and 3-4 respectively. From these plots a user can determine the wing twist and vertical bending at any point along the span. The program code can be found in the Appendix.

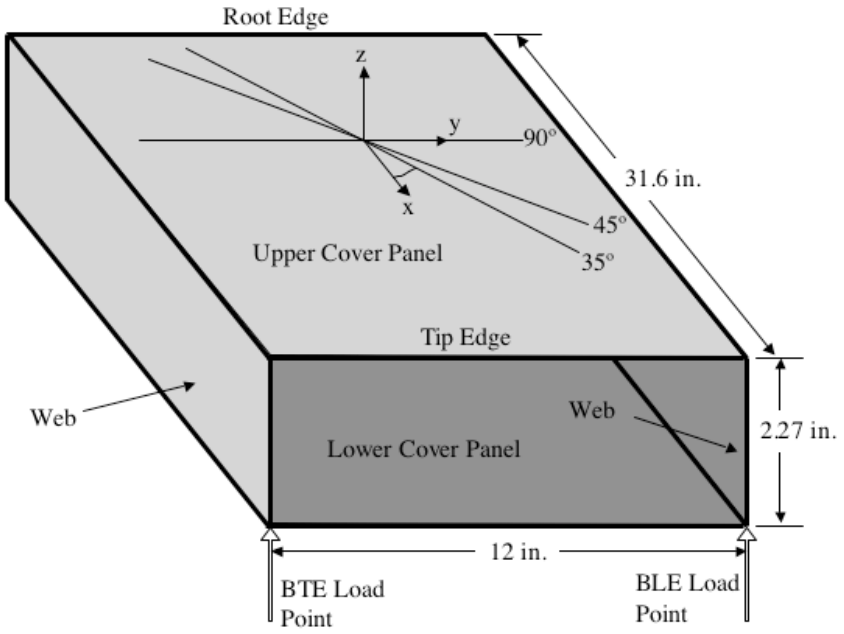

Figure 3-2: Closed Form Code Model

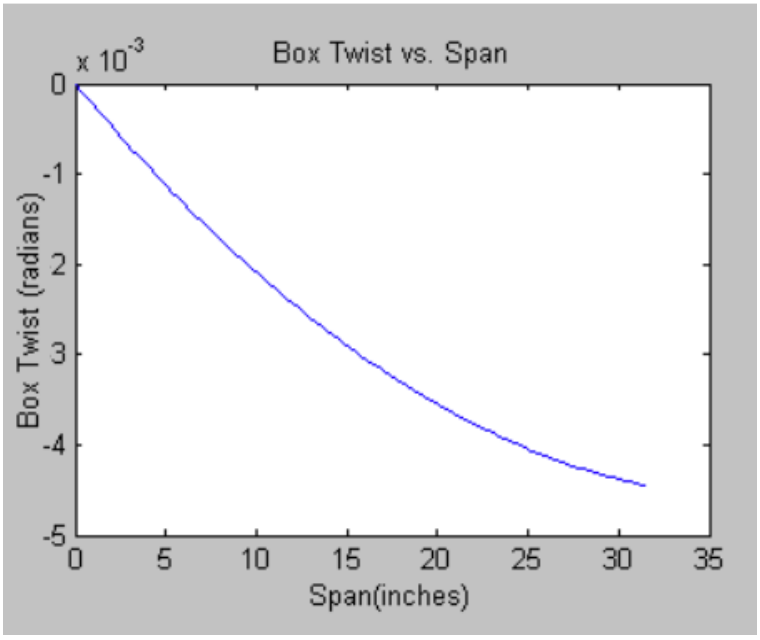

Figure 3-3: CFC Output – Box Twist vs. Span

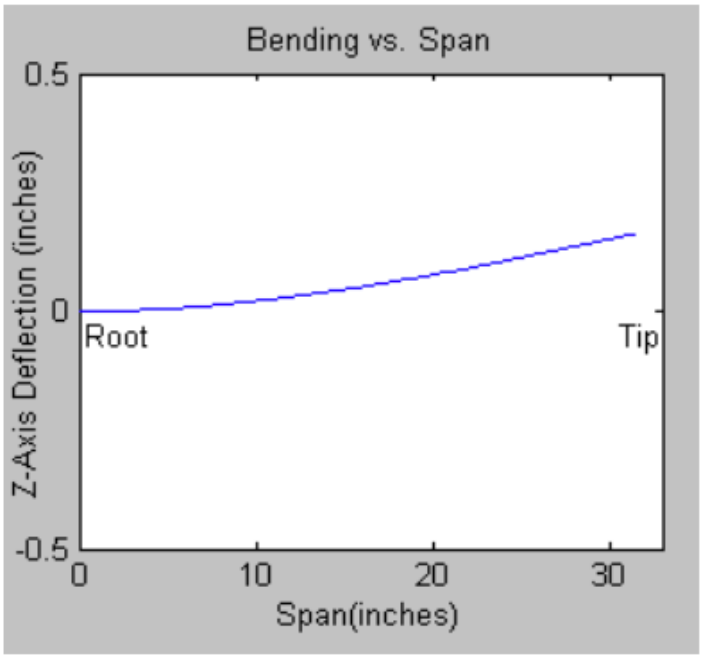

Figure 3-4: CFC Output – Bending vs. Span

3.1.2 CFC Wing Box Analysis

The Matlab Aeroelasticity program was used to perform an analysis of the wing box final design. The program input requires material properties, stacking sequence and thickness of each panel, and the load condition. The material properties and geometry of the final wing box design are shown in Tables 3-1 and 3-2.

Table 3-1: Ply Properties of IM7 Fiber/VR56-19 Resin

Property	*Value (psi)*
E_{11}	20.1×10^6
E_{22}	1.47×10^6
G_{12}	1.53×10^6
ν_{12}	0.31

Table 3-2: Panel Geometry

Panel	*Stacking Sequence*	*Thickness*	*Dimension*
Upper Cover	$[35/90/35/(45/90)_2]_s$	0.086 in.	12 x 31.6 in.
Lower Cover	$[-35/90/-35/(-45/90)_2]_s$	0.086 in.	12 x 31.6 in.
Trailing Web	$[\pm 45]_s$	0.050 in.	2 x 31.6 in.
Leading Web	$[\pm 45]_s$	0.050 in.	2 x 31.6 in.

The upper and lower cover panels are identical except that the angle plies in the stacking sequence are opposite in sign. The CFC model in Figure 3-2 illustrates the box coordinate system, of which the z-axis always points outward from the box panel. Therefore to represent the required orientation, the angle plies must be positive on the upper cover and negative on the lower cover panel.

The specimen is loaded individually at two locations. The first location is at the Bottom Trailing Edge corner at the wing tip. This point is designated as the BTE corner. Similarly the

second location is at the Bottom Leading Edge (BLE) corner on the wing tip as shown in Figure 3-2. Since it is difficult to load the box specimen exactly on the wing tip, the actual load points are located 0.4 inches inboard from the tip. To adjust for this change the wing box length was analyzed as 31.6 inches as opposed to the full 32 inches of the box. The analysis was applied to each load case.

While this analysis using the closed form code is relatively quick and simple, it has a few drawbacks. The CFC is unable to consider complex parts. A real wing box specimen requires fixtures to hold the panels together and to secure it to the test wall. These extra parts add stiffness and imperfections to the structure that are not considered by the closed form analysis. In addition, the CFC is unable to predict local deformations that could affect the global behavior of the structure. Therefore this form of analysis is useful only for the early stages of design work and is not suitable for a refined analysis.

3.2 Finite Element Analysis

The finite element analysis (FEA) was used for two purposes. First, in the specimen design phase, the FEA was used to aid in achieving the design goals set for the wing box specimen. Second, the analysis was used to predict the behavior of the actual specimen. The finite element model was refined to account for measured specimen dimensions and the added stiffness due to the presence of angle brackets and other fixtures used to assemble the box. Pre and post processing of the model was performed in PATRAN[11] and STAGS[12] was used as the finite element solver.

3.2.1 Linear Analysis

The finite element model represents the geometry of the assembled carbon fiber panels. The cover panels are 14 x 32 inches and the web panels are 2.27 x 32 inches as shown in Figure 3-5. Each finite element is a STAGS 410 quadrilateral with 4 nodes[12]. Since the area near the brackets have more complexity, the mesh on the cover panels was applied with a 2 way bias across the width of the box. An L2/L1 ratio of 5 was used to define the bias as shown in Figure 3-6. The span-wise edge length was limited to a maximum of 0.40 inches and the web element height was limited to 0.20 inches. The total model contains 6,560 elements with 39,852 degrees of freedom. The elements were defined as shells and assigned the panel properties that are listed in Table 3-4. The ply properties used for the carbon fiber layers are the same as in Table 3-1. To compensate for the stiffness added by the angle brackets, the web and cover panel thicknesses were increased in the appropriate areas. Eccentricity was accounted for in these thickened sections by adding an offset to define the mid-plane.

Table 3-3: Finite Element Model Shell Geometry

Property Set	*Stacking Sequence*	*Thickness*	*Eccentricity*
Upper Cover	$[35/90/35/(45/90)_2]_s$	0.086 in.	0 in.
Lower Cover	$[-35/90/-35/(-45/90)_2]_s$	0.086 in.	0 in.
Web	$[\pm 45]_s$	0.050 in.	0 in.
Lower Cover/Carbon Bracket	$[-35/90/-35/(-45/90)_2]_s/[\pm 45]_s$	0.156 in.	-0.035 in.
Carbon Bracket/Upper Cover	$[\pm 45]_s$ /$[35/90/35/(45/90)_2]_s$	0.156 in.	0.035 in.
Web/Carbon Bracket	$[\pm 45]_s/[\pm 45]_s$	0.120 in.	0.035 in.
Carbon Bracket/Upper Cover/Aluminum Bracket	$[\pm 45]_s$ /$[35/90/35/(45/90)_2]_s$/Al	0.2185 in.	0.0038 in.
Aluminum Bracket/Web/Carbon Bracket	Al/$[\pm 45]_s/[\pm 45]_s$	0.1825 in.	0.0038 in.
Aluminum Bracket	Al	0.0625 in.	-0.0563 in.

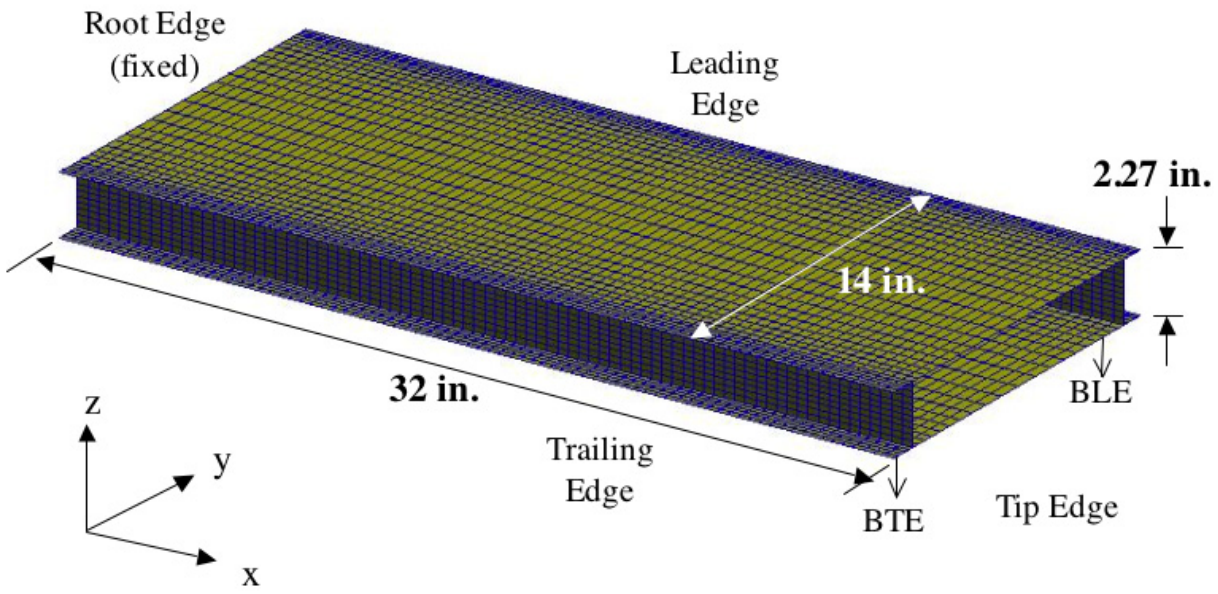

Figure 3-5: Finite Element Wing Box Model

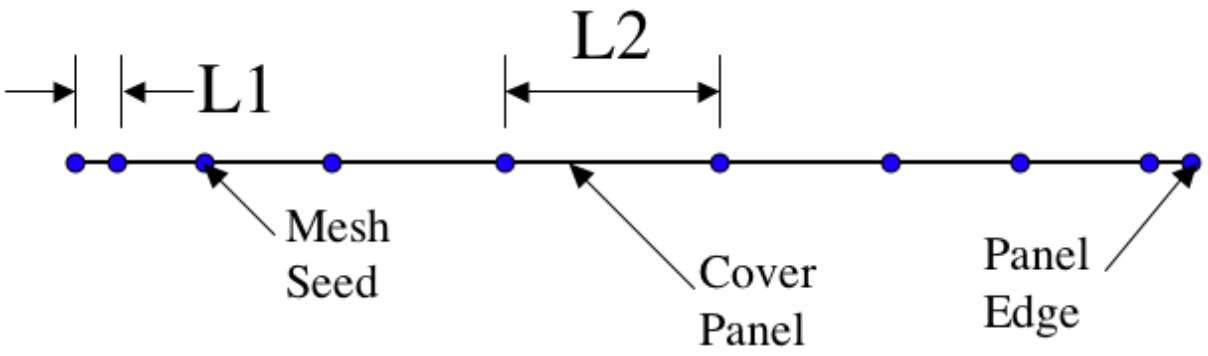

Figure 3-6: Finite Element Mesh Bias

One inch of the root end of the wing box is potted with a resin mixture. To apply the boundary conditions induced by the potting, all nodes along the root edge of the finite element model are restrained in all directions and rotations. As with the closed form analysis two loading

locations are considered in the FEA. Load is applied to the BTE corner and the BLE corner independently.

3.2.2 Failure Analysis

A failure analysis was conducted to verify that the specimen would not fail prematurely and to predict the failure mode. A first ply failure technique was used for the analysis. Failure loads were determined using the maximum stress criterion. The properties used in the analysis are listed in Table 3-4. The axial tension strength, X_t, is a property given by Hexcel Composites. Transverse compression strength, Y_c, and shear strength, S, are taken from the VARTM resin data sheet by Applied Poleramic Inc. Properties were not available for axial compression, X_c, and transverse tension, Y_t, so nominal values for carbon/epoxy were used[8].

Table 3-4: IM7/VR56-19 Ultimate Strength Properties

Property	*Reference*	*Value (psi)*
X_t	13	*400000
X_c	8	150000
Y_t	8	6000
Y_c	14	103000
S	14	17000

*Note: Typical fiber/resin strength for 12K filament count

The failure stress of a ply given the angle between the fiber and the load is shown in Figure 3-7. The solid line indicates the maximum stress in tension and the dashed line indicates compression failure. Using this plot, one can compare each ply stress to its failure stress. The failure stresses pertinent to the plies of wing box cover panels are summarized in Table 3-5.

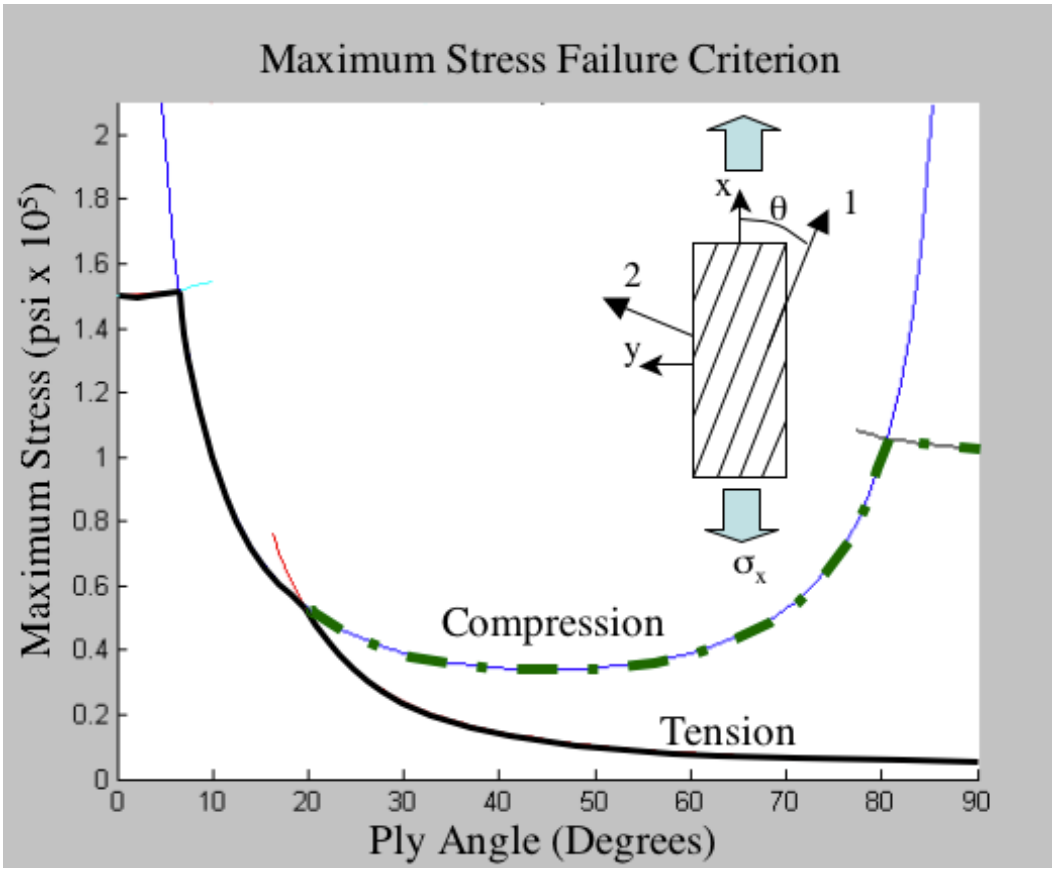

Figure 3-7: Ply Failure Plot

Table 3-5: Relevant Ply Strengths

Fiber Angle	*Tension Failure (psi)*	*Compression Failure (psi)*
0°	150000	150000
35°	18000	36000
45°	12000	34000
55°	8000	36000
90°	6000	103000

The finite element solver can resolve the stress in each ply of the laminates. These ply stresses were evaluated for both load sets. Both σ_{xx} and σ_{yy} were considered for each ply in the box and checked against the appropriate failure stress. The ply that has the lowest factor of safety

(stress limit to ply stress ratio) will be the first ply to fail. Since the strength of the plies in compression is much greater than in tension, the lower cover panel is the most critical region of the box. The lowest factors of safety shown in Table 3-6 occurred during the BTE load in the x-direction (σ_{xx}). In this case the 35° ply #14 of the lower cover panel would be the first to reach its failure stress. Since the FEA is linear, the failure load can be found simply by multiplying 100 lb by ply fourteen's factor. Based on the maximum stress criterion ply 14 of the lower cover panel is predicted to fail at approximately 225 lb to 230 lb, so the wing box specimen should not fail during test loads.

Table 3-6: Lower Cover Panel Axial Ply Stresses Under BTE Load

Ply	*Fiber Angle*	*Ply Stress (psi)*	*Stress Limit (psi)*	*Factor of Safety*
1	35	7090	18237	2.57
2	90	1390	6000	4.32
3	35	7240	18237	2.52
4	45	4030	12000	2.98
5	90	1380	6000	4.35
6	45	4170	12000	2.88
7	90	1480	6000	4.05
8	90	1550	6000	3.87
9	45	4370	12000	2.75
10	90	1430	6000	4.20
11	45	4500	12000	2.67
12	35	7880	18237	2.31
13	90	1400	6000	4.29
14	35	8020	18237	2.27

Another possible failure mode is failure of the bond between the brackets and web or cover panels. FEA results indicated that the trailing edge root had the highest shear stress of either load case. However insufficient information is available concerning the adhesive

properties. While the adhesive failure could not be predicted, it was not expected to occur during the test loads.

The forces introduced to the specimen corners induce compressive loads into the upper cover panel. A linear buckling analysis was applied to the finite element model to determine if buckling would occur in the test load range. STAGS did not find any critical loads between 0 and 250 lb when applied to the BTE or BLE corners, so panel buckling was not expected to occur prior to box failure.

Chapter 4 : Wing Box Test

The small-scale wing box that was designed and analyzed using methods described in Chapter 3 was fabricated and tested at the NASA Langley Research Center. Facilities operated by the Mechanics and Durability Branch were used to perform the test. The data obtained from the experiment is used in Chapter 5 for analysis validation.

4.1 Instrumentation

Twenty-four back-to-back strain gages were used to measure wing box behavior. Two sets of axial gages were placed along the root of each cover panel, measuring strain in the x-direction. Strain rosettes measuring strain at 0°, 45°, and 90° were placed near the center of each cover panel and along the wing tip. The gage layout for the cover panels is shown in Figure 4-1. Both web panels had mid-span axial gages aligned at 0° and one aligned at 90° to the x-axis

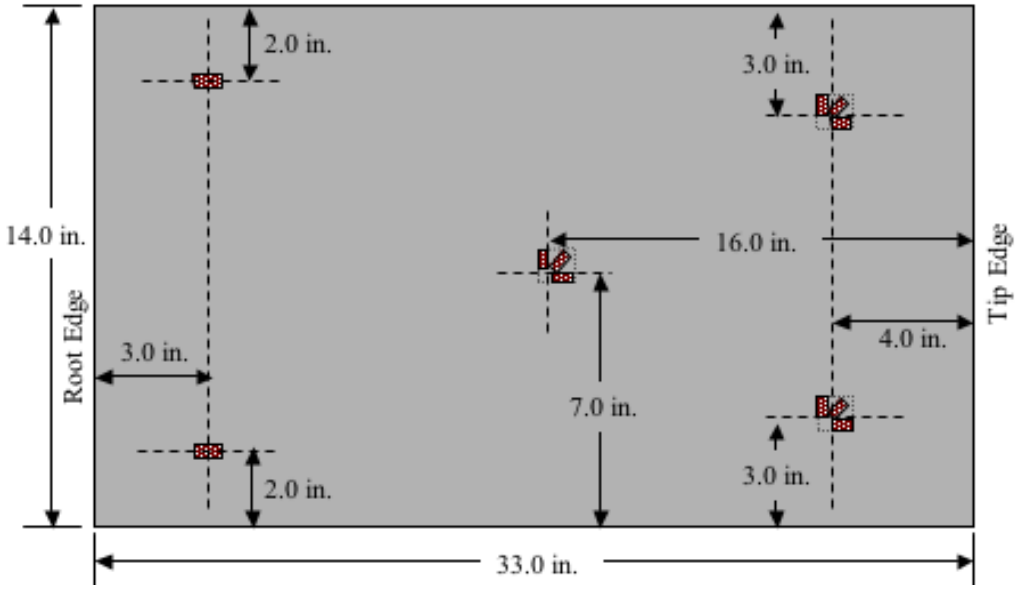

Figure 4-1: Cover Panel Strain Gage Layout

Eleven Direct Current Displacement Transducers (DCDT's) were distributed on the wing box and potting to measure displacement as shown in Figure 4-2. Four of these DCDT's were placed along the tip edge of the box (Figure 4-3) and two more were placed mid-span along the box on the leading and trailing edge (Figure 4-4). These transducers were calibrated assuming a maximum of 0.5-inch stroke.

Five more displacement transducers were placed on the potting with a 0.01 inch maximum stroke to determine if the potting and root edge was indeed fixed as assumed in the analyzes. Transducer 58 and 71 are on the trailing edge side of the potting as shown in Figure 4-5. Transducer 71 measures the movement of the potting away from the test wall, or backstop, on the trailing edge. Similarly transducer 74 measures the movement on the leading edge side. Displacement transducers 72 and 73 are underneath the potting to measure any sliding of the potting on the backstop as seen in Figure 4-6. During the last 3 trials, displacement transducer 73 was moved from the potting to the root of the lower cover to measure any deflection of the panel at the base of the potting (Figure 4-7). A summary of all transducers is shown in Table 4-1.

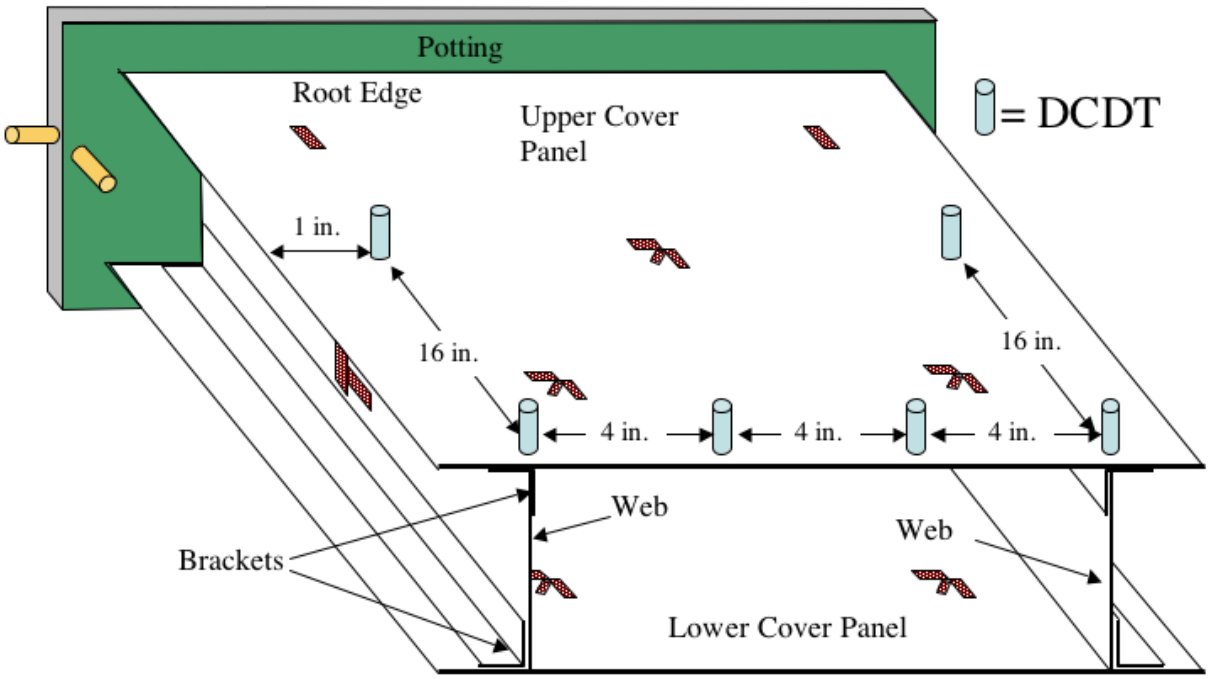

Figure 4-2: DCDT Layout

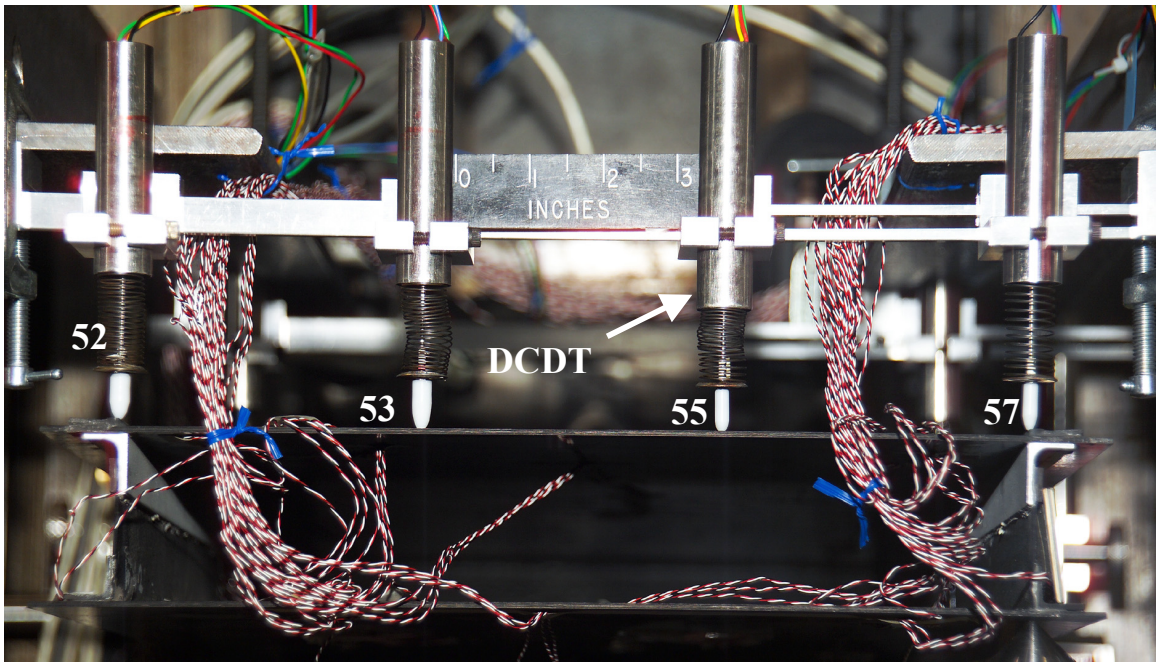

Figure 4-3: Tip DCDT's

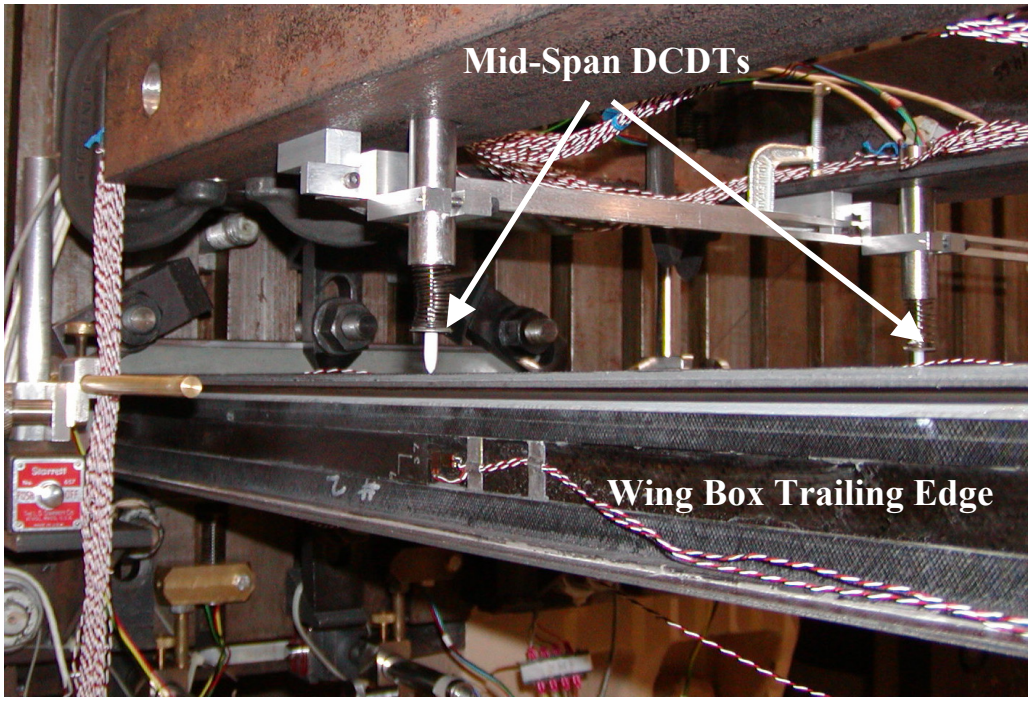

Figure 4-4: Mid-Span DCDTs

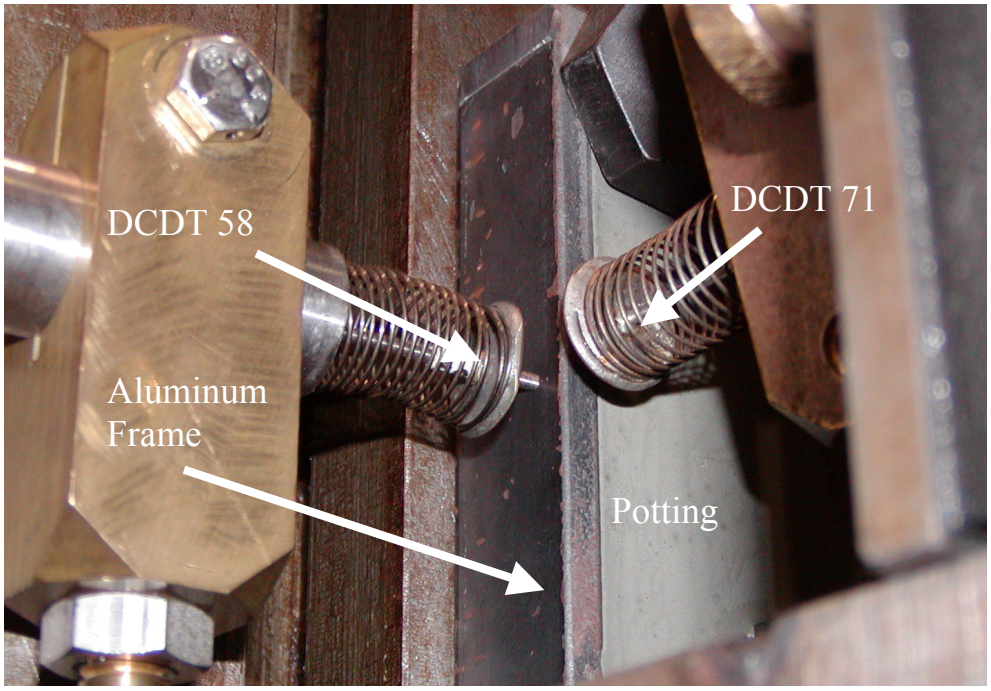

Figure 4-5: Trailing Edge Potting DCDT's

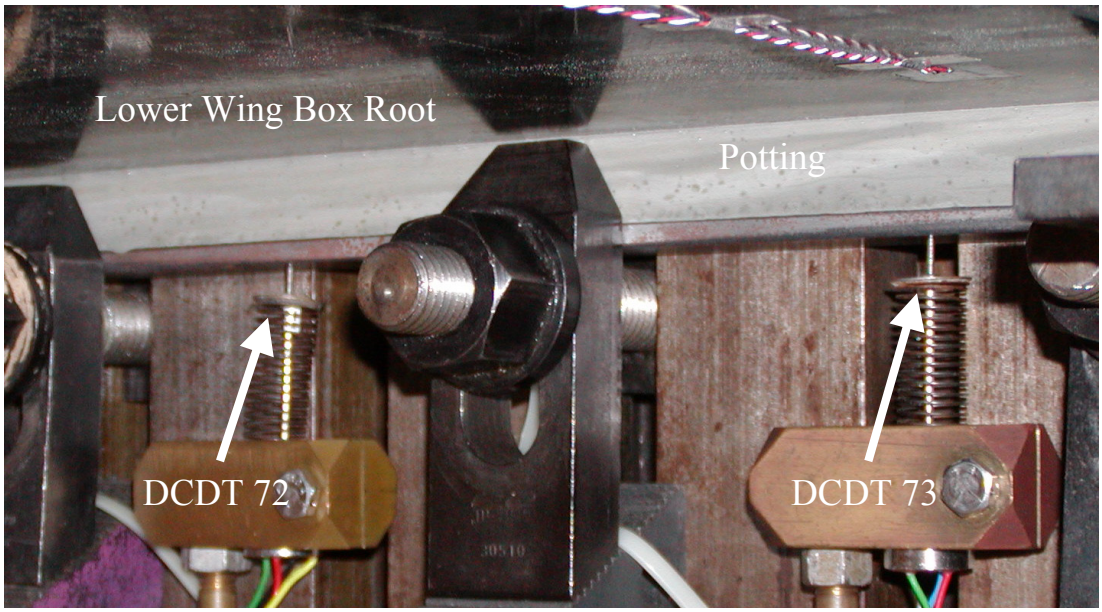

Figure 4-6: Bottom Potting DCDT's

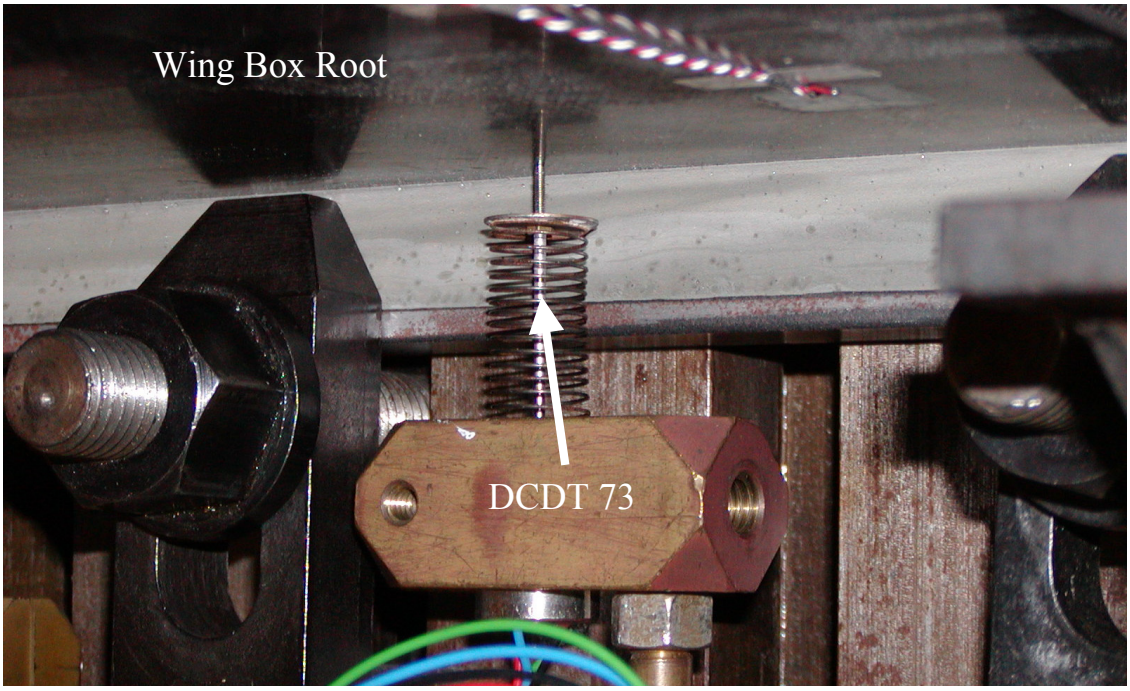

Figure 4-7: Panel Root DCDT

Table 4-1: List of Instrumentation

Transducers			
#	*Type*	*Box Region*	*Location*
1-2	Strain: axial	Upper Cover	Trailing edge, root
3-4	Strain: axial	Upper Cover	Leading edge, root
7-8	Strain: rosette	Upper Cover	Center, mid-span
11-12	Strain: rosette	Upper Cover	Trailing edge, tip
15-16	Strain: rosette	Upper Cover	Leading edge, tip
17-18	Strain: axial	Lower Cover	Leading edge, root
19-20	Strain: axial	Lower Cover	Trailing edge, root
23-24	Strain: rosette	Lower Cover	Center, mid-span
27-28	Strain: rosette	Lower Cover	Leading edge, tip
31-32	Strain: rosette	Lower Cover	Trailing edge, tip
33-34	Strain: axial	Web	Leading edge, mid-span
35-36	Strain: transverse	Web	Leading edge, mid-span
37-38	Strain: axial	Web	Trailing edge, mid-span
39-40	Strain: transverse	Web	Trailing edge, mid-span
50	DCDT: 0.5 inch	Upper Cover	Trailing edge, mid-span, Z-Disp.
51	DCDT: 0.5 inch	Upper Cover	Leading edge, mid-span, Z-Disp.
52	DCDT: 0.5 inch	Upper Cover	Trailing edge, tip, Z-Disp.
53	DCDT: 0.5 inch	Upper Cover	Trailing edge + 4 inches, tip, Z-Disp.
55	DCDT: 0.5 inch	Upper Cover	Trailing edge + 8 inches, tip, Z-Disp.
57	DCDT: 0.5 inch	Upper Cover	Leading edge, tip, Z-Disp.
58	DCDT: 0.001 inch	Potting	Trailing edge, Y-Disp.
71	DCDT: 0.001 inch	Potting	Trailing edge, X-Disp.
72	DCDT: 0.001 inch	Potting	Bottom, Z-Disp.
73	DCDT: 0.001 inch	Potting/Lower Cover	Bottom, Z-Disp.
74	DCDT: 0.001 inch	Potting	Leading edge, X-Disp.

4.2 Test Setup and Procedure

The wing box was secured to a test wall using several clamps as shown in Figure 4-8. A hydraulic actuator was positioned underneath the tip end of the wing box to apply the load. This actuator was attached to a steel plate with clamps to allow easy movement between the two load points. The actuator was controlled using a hand pump. Load was measured by a 300-lb capacity load cell attached to the top of the actuator arm. A rod with a blunt nosed cone was threaded into the load cell for load introduction as shown in Figure 4-9.

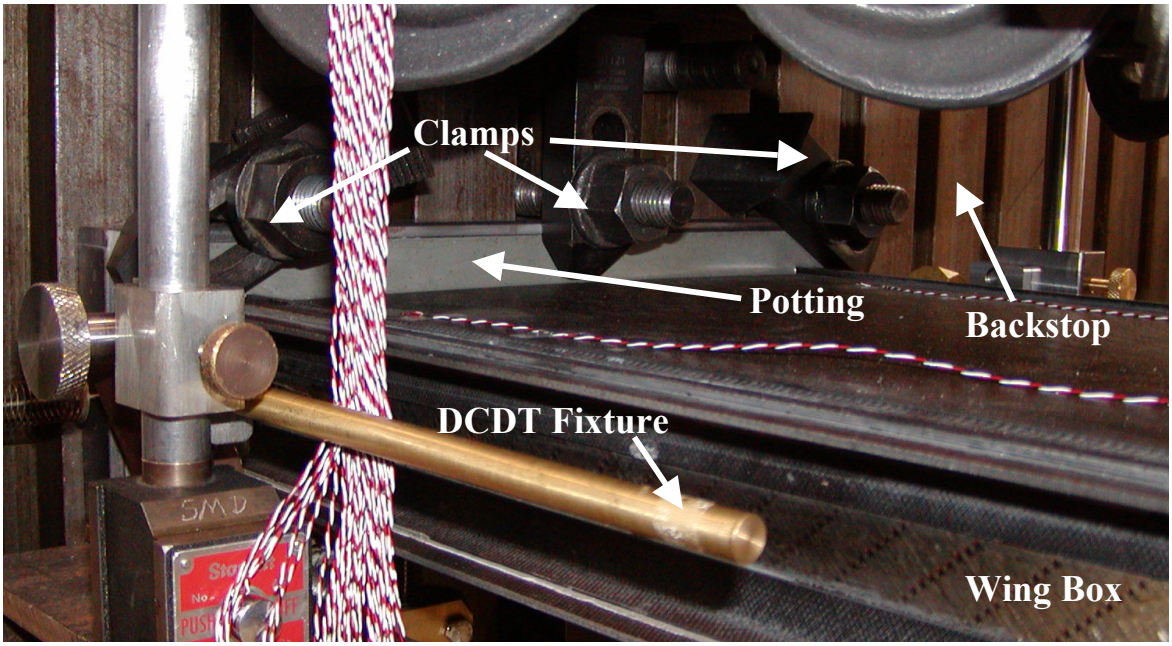

Figure 4-8: Clamped Root End

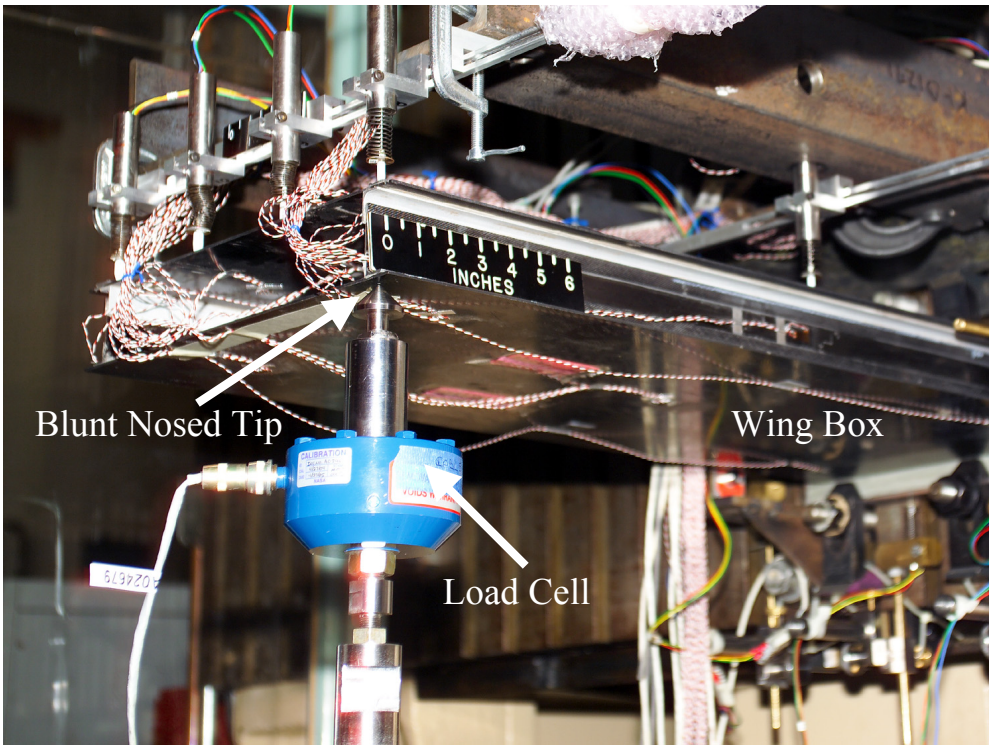

Figure 4-9: Load Introduction

For each test, the actuator was positioned underneath either the BTE corner or the BLE corner. The load was introduced to a point 0.4 inches inboard from the tip (31.6 inches from wing root) as analyzed. A level was used to verify that the actuator would apply a vertical load. Prior to beginning a trial, the DCDT and strain gage signals were set to zero and the system began to record data at the rate of 1 scan per second. The hand pump was used to apply the load at approximately 1 to 2 lb/sec. Once the desired load was achieved, it was held for 10 seconds to allow the system to settle. Data was recorded throughout the hold to verify that there was no significant change in load. The wing box specimen was photographed in its deformed position at this time. After the hold period the load was released. During the last trial, the specimen was loaded to failure with the load introduced at the bottom trailing edge corner. The test sequence is listed in Table 4-2.

Table 4-2: Test Sequence

Run #	*Load Point*	*Max Load (lb)*
1	BTE	20
2	BLE	20
3	BLE	50
4	BTE	50
5	BTE	80
6	BLE	80
7	BLE	100
8	BTE	100
9	BTE	Failure

The transducers measuring displacements of the potting or root area were monitored during each test. Throughout the trials these displacements were on the order of 10^{-5} inches. These readings reinforced the assumption that the setup represented a cantilever beam. DCDT 73

was placed underneath the root of the lower cover panel to quantify any movement within the potting. The measured deflections at this location were negligible.

Chapter 5 : Discussion of Results

This chapter compares the predicted results from the analyses to the measured values from the experiment. Displacement and strain results from the finite element analysis are directly compared to the response of the wing box. The twist and bending of the wing box specimen is calculated for comparison to the closed form code results. Unless otherwise specified, percent errors are calculated based on the measured value.

5.1 Finite Element Analysis

There was good correlation between the finite element results and the measured displacements. Predicted deflections at the tip DCDT locations and the measured values for the two 100 lb load cases are shown in Table 5-1. For the most part the analysis predicts the upper cover panel displacement to within 5-6%. The exception occurs at displacement transducer 57 during the BTE load case and transducer 52 during the BLE load case. Here the error between the FEA and the test results is 13-15 %. These locations with the larger error correspond to the transducers above the web opposite to that being loaded (i.e., when the corner directly below DCDT 52 is being loaded, DCDT 57 has a larger error). This error is likely an effect of the accuracy limitations of the displacement transducer. Transducer 57 in the BTE load case is 0.032 inches while the predicted value is 0.028 inches. The difference is 0.004 inches out of a full-scale range of 0.5 inches. The transducer error is to be 0.5% of the full-scale range or ±0.0025 inches. The mid-span transducers (50 and 51) predict the trend of the wing box specimen but also

encounter high error due to small displacements. At higher deflections, the finite element analysis results in a maximum error of 7%.

Table 5-1: Comparison of Tip Displacements

		100 lb BTE Load			100 lb BLE Load		
Location	*DCDT*	*Predicted Disp. (in.)*	*Measured Disp. (in.)*	*Error*	*Predicted Disp. (in.)*	*Measured Disp. (in.)*	*Error*
Tip	52	0.219	0.233	6%	0.028	0.033	15%
	53	0.183	0.197	7%	0.044	0.043	2%
	55	0.085	0.090	6%	0.124	0.124	0%
	57	0.028	0.032	13%	0.163	0.171	5%

Note: Error based on measured value

The measured and FEA predicted values for the deflection of the upper cover panel at 100 lb load in BTE and BLE locations are shown in Figures 5-1 and 5-2 respectively. The plots show that the actual wing box specimen deflected slightly more than predicted by the analysis. This behavior indicates that the finite element model is slightly stiffer than the actual specimen.

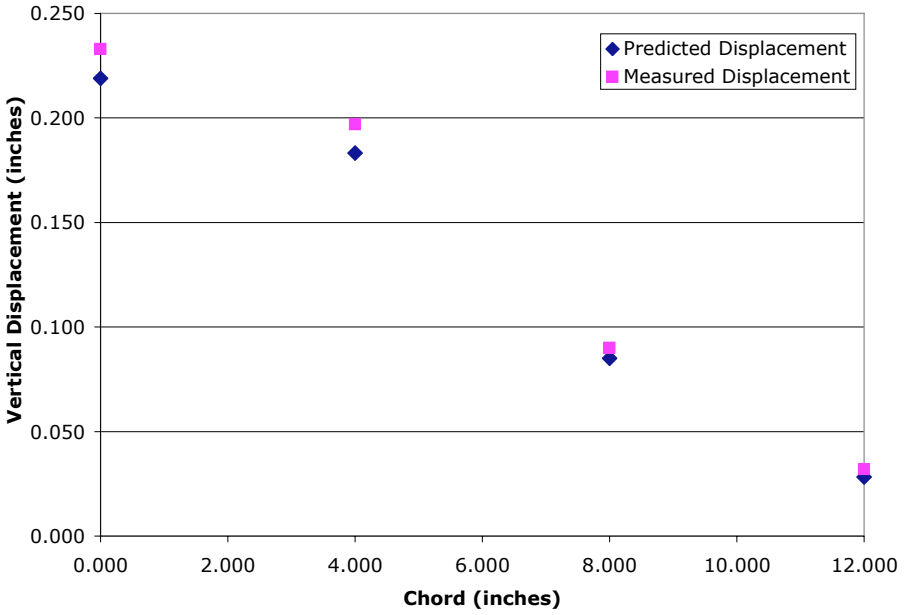

Figure 5-1: Measured and Predicted Displacements for 100 lb BTE Load

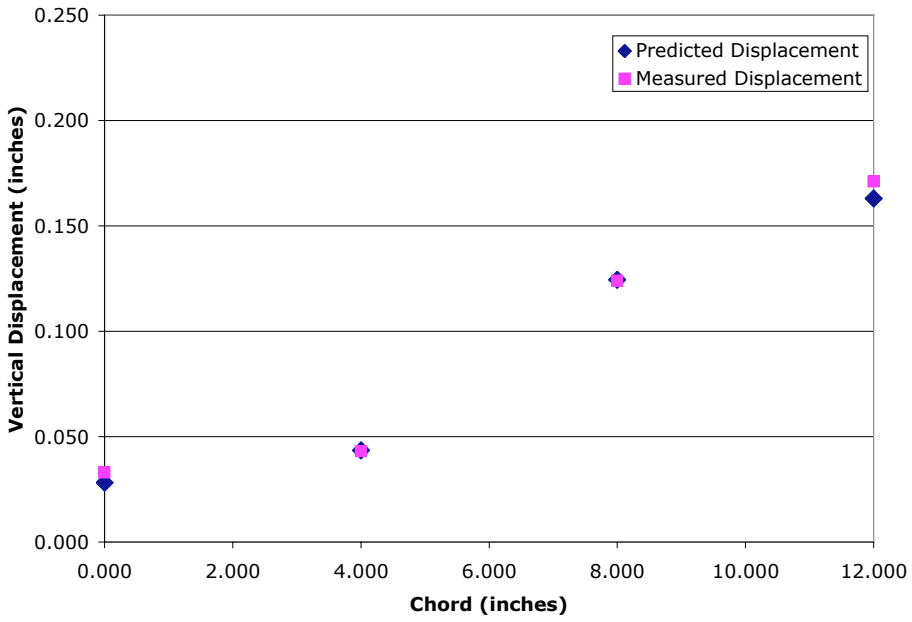

Figure 5-2: Measured and Calculated Displacements for 100 lb BLE Load

An interesting feature to note is the curve along the tip of the cover panels. A deformation plot of the wing box with a 100 lb BLE load is shown in Figure 5-3. In this figure the deformation is magnified by ten. The bending of the cover panels takes the shape of a flattened S-curve along the tip. Figure 5-4 is a picture of the box specimen under load. If the upper cover panel is inspected closely, the S-curve can be seen in the specimen. The finite element model has the capability to predict the camber curvatures of the wing box.

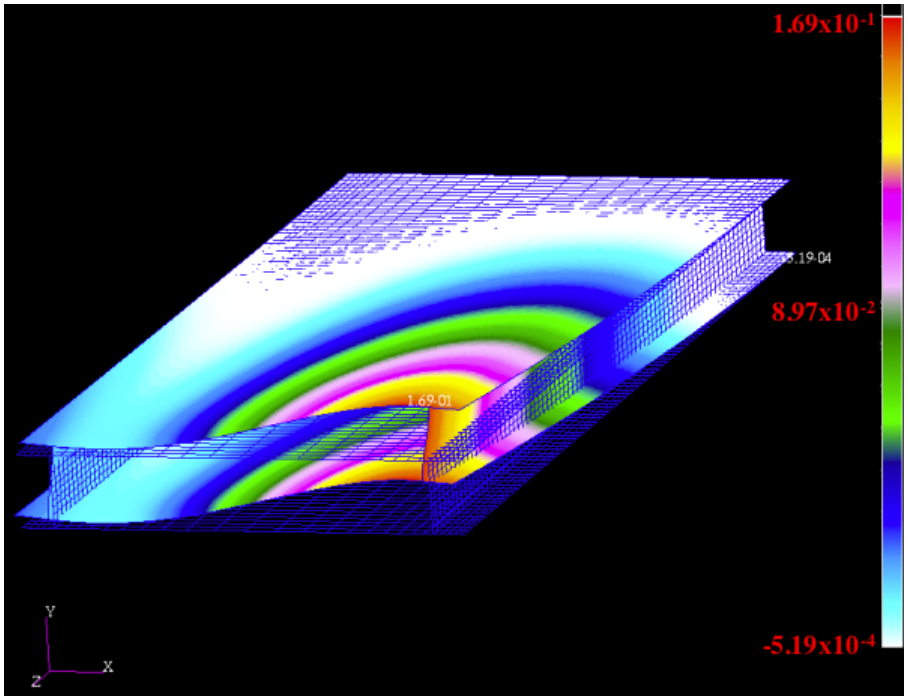

Figure 5-3: FEA Deformation Plot (100 lb BLE Load)

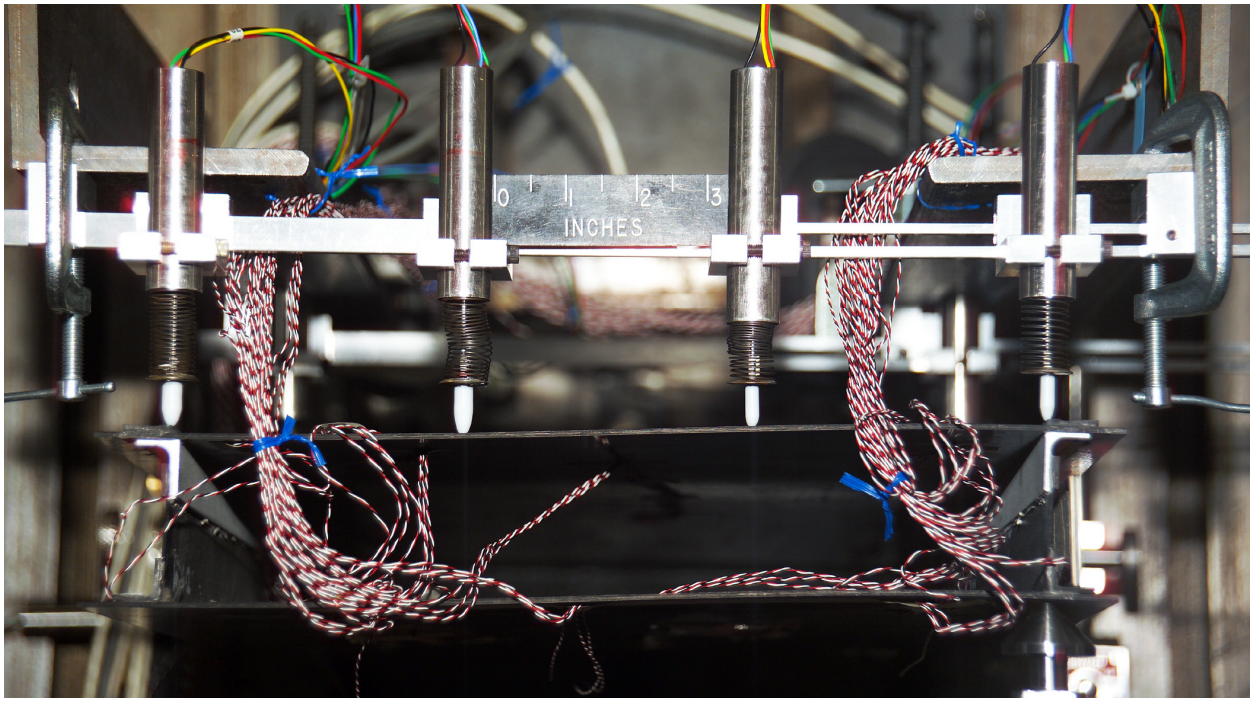

Figure 5-4: Camber Curvature during 100 lb BLE Load

The predicted axial strains along with the measured strains from the wing box root are listed in Table 5-2. The error based on the measured value ranges from 1% to 15%. Gages on the trailing edge side (# 1-2, 17-18) have smaller errors than the gages on the leading edge side (# 3-4, 19-20).

Table 5-2: Wing Box Root Axial Strains

	100 lb BTE Load					100 lb BLE Load			
		Strain (με)					*Strain (με)*		
	Gage #	*Analysis*	*Measured*	*Error*		*Gage #*	*Analysis*	*Measured*	*Error*
Root Gages	1	-514	-484	6%	Root Gages	1	-163	-157	4%
	2	-465	-448	4%		2	-155	-146	6%
	3	-175	-152	15%		3	-411	-371	11%
	4	-161	-143	13%		4	-376	-344	9%
	17	642	637	1%		17	182	175	4%
	18	685	641	7%		18	189	177	7%
	19	203	190	7%		19	496	457	9%
	20	219	202	8%		20	534	487	10%

Difficulties occur in the comparison since the strain gradient is steep in this specimen. An element near the root of the finite element model, shown in Figure 5-5, illustrates the interpolated strain range over a 0.400-inch by 0.416-inch area. The strain in the element has a 26 με range, which is 15.3% of the largest value on the element. Any imperfections in the boundary conditions or panels of the wing box specimen can shift the strain gradient causing a larger error when compared to the FEA predicted strains. The dashed line in Figure 5-5 indicates the relative size of the axial strain gages. A direct comparison of strain results and analysis is problematic since the gages measure an average strain over an area rather than a point.

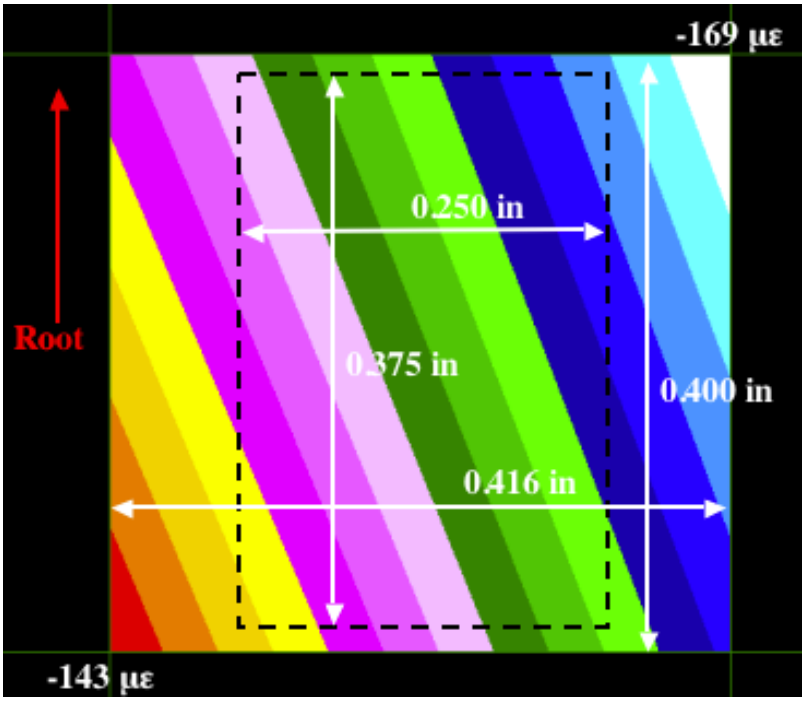

Figure 5-5: Wing Root Element Strain Gradient

The predicted and measured strain results are normalized with respect to the highest strain in the set (i.e., the analyzed strain for the 100 lb BTE load was normalized to 685 microstrain). The error based on the normalized measured strains is listed in Table 5-3.

Table 5-3: Wing Box Root Normalized Axial Strains

	100 lb BTE Load					100 lb BLE Load			
		Strain (με)					*Strain (με)*		
	Gage #	*Analysis*	*Measured*	*Error*		*Gage #*	*Analysis*	*Measured*	*Error*
Root Gages	1	-0.750	-0.755	1%	Root Gages	1	-0.305	-0.322	5%
	2	-0.679	-0.699	3%		2	-0.290	-0.300	3%
	3	-0.255	-0.237	8%		3	-0.770	-0.762	1%
	4	-0.235	-0.223	5%		4	-0.704	-0.706	0%
	17	0.937	0.994	6%		17	0.341	0.359	5%
	18	1.000	1.000	0%		18	0.354	0.363	3%
	19	0.296	0.296	0%		19	0.929	0.938	1%
	20	0.320	0.315	1%		20	1.000	1.000	0%

The errors of the predicted normalized values with respect to the measured normalized values are less than 8%. The FEA is able to predict the strain trends of the wing box specimen. It is likely that the finite element analysis would perform well in predicting the behavior of a full-scale tailored structure. The percentage error of the predicted results would be expected to decrease with a larger specimen and higher loads.

The axial strains measured by the five gages on the outer side of the lower cover panel and the predicted values when loaded at 100 lb BTE load are plotted in Figure 5-6. The dashed line indicates the measured values and the solid line indicates the predicted values. In general the predicted values are higher than the measured values. However the strain trends are predicted indicating that the finite element model represents the overall box stiffness well.

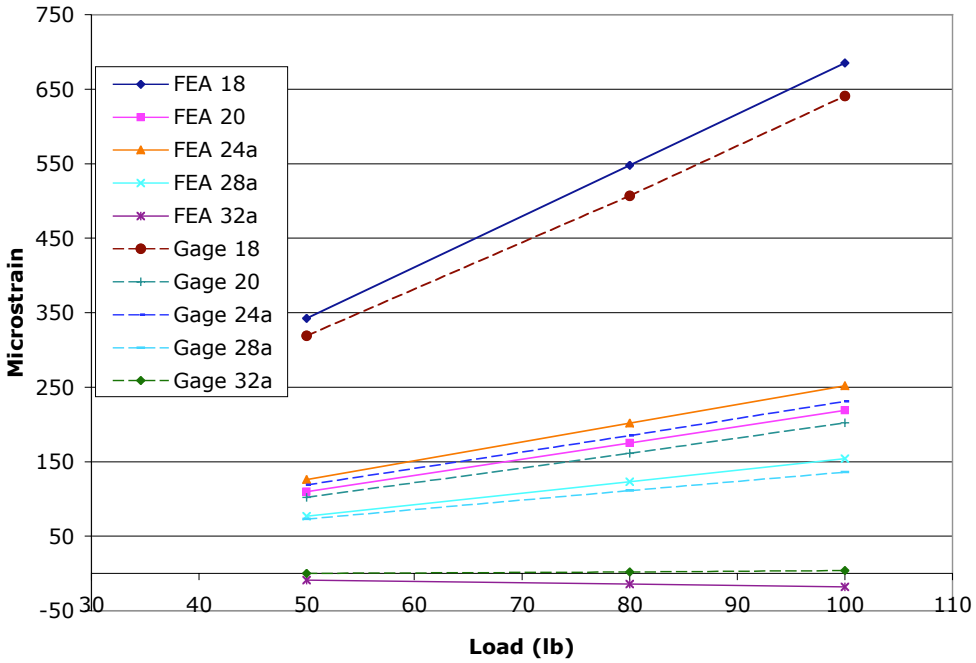

Figure 5-6: Lower Cover Panel Strain Trends

The strain measurements can be used to determine the presence of axial panel bending. Back-to-back upper cover panel strains associated with the 100 lb load cases are listed in Table 5-4. The percent axial bending relative to extension can be determined by the equation $B = \frac{|\varepsilon_t - \varepsilon_b|}{|\varepsilon_t + \varepsilon_b|} \times 100$ were ε_t is the measured strain on the top of the panel, ε_b is the strain on the bottom, and B is the percent bending[10]. Near the root and at the center of the panel the bending is small. However the percent bending is 20%-60% at the tip gage closest to the load introduction and over 200% at the tip gage farthest from the load. While the strains are small near the tip, strain due to bending is more significant strain due to extension.

Table 5-4: Axial Bending in Upper Cover Panel for 100 lb BTE Load

	100 lb BTE Load			100 lb BLE Load		
Upper Cover Location	*Top Gage (με)*	*Bottom Gage (με)*	*% Bending*	*Top Gage (με)*	*Bottom Gage (με)*	*% Bending*
Trailing Edge Root	-484	-448	4%	-157	-146	4%
Leading Edge Root	-152	-143	3%	-371	-344	4%
Center Mid-span	-189	-186	1%	-118	-136	7%
Trailing Edge Tip	-107	-72	20%	10	-23	254%
Leading Edge Tip	-12	30	233%	-15	-61	61%

5.2 Failure

The first noticeable sign of box failure occurred at a load of 231 lb at the BTE corner by a significant drop in load. This failure took place at the leading edge tip through a delamination between the aluminum bracket and the upper cover panel as shown in Figure 5-7. After unloading the specimen, the panels were visually checked for any damage. There is no surface evidence of any laminate failure on any of the panels.

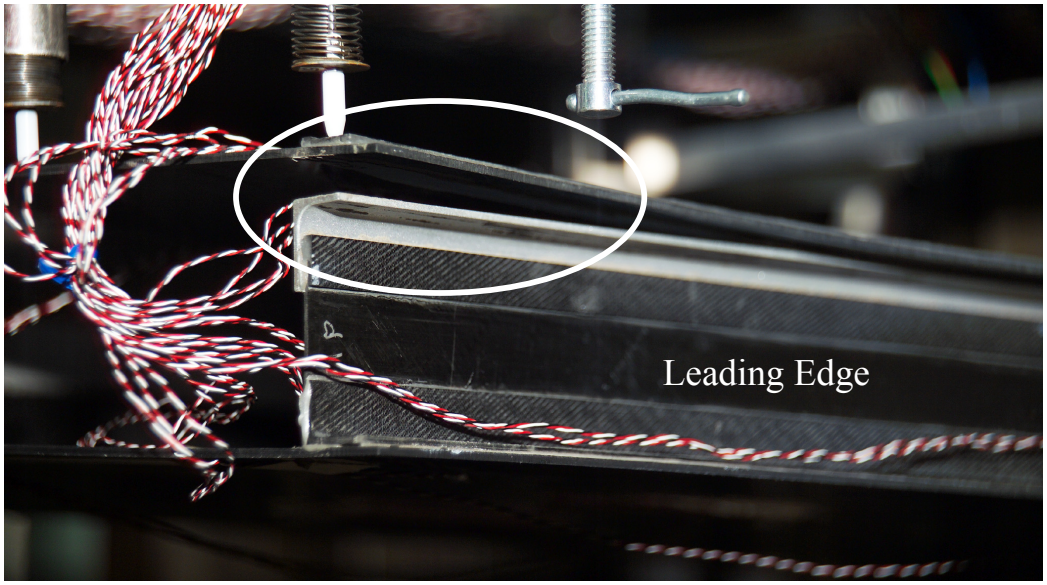

Figure 5-7: Bracket/Panel Delamination

The finite element analysis indicated that the peak bond shear stress was near the trailing edge root. However no visual delamination could be found in that region prior to the leading edge bond failure. As seen in Figure 5-8, the upper cover panel appears to be peeling away from the bracket. The bond failure was probably induced by a combination of peeling and shear.

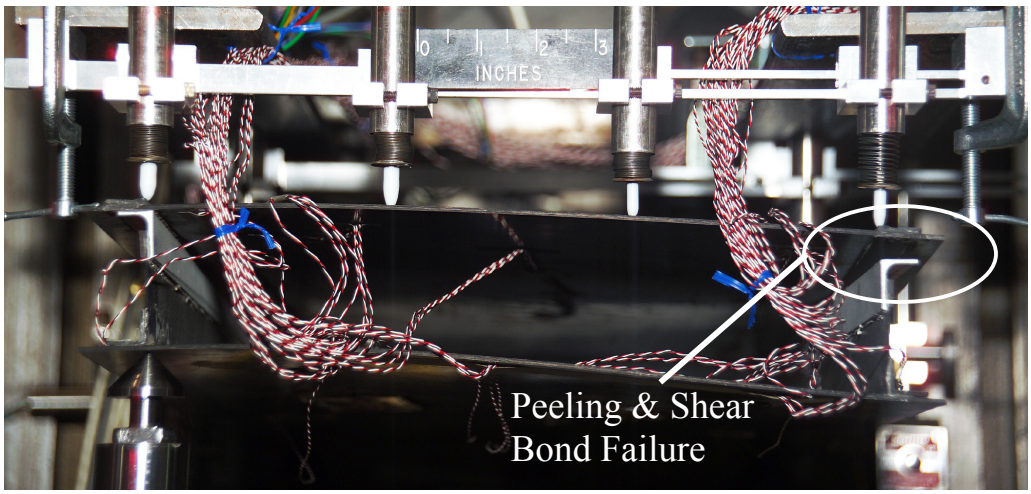

Figure 5-8: Bond Shear/Peeling Failure

5.3 Closed Form Code

Since the closed form code can only predict twist and bending as a function of span, the output from the FEA and test had to be converted to a similar form for comparison. The magnitude of twist and bending at the wing tip is estimated from the vertical displacements of the FEA model and the test specimen. A line drawn between the upper corners of the deformed wing box represents the upper cover panel without any out-of-plane deformation. The vertical displacement of the mid-point is considered to be the tip bending and the slope of the line is used to find the twist.

The closed form code is only partially successful in its prediction of the tailored wing box. The measured and predicted bend and twist results for the BTE load case are listed in Table 5-5 and corresponding error based on the measured value is in Table 5-6. The results from the BLE load case are listed in Table 5-7 and the corresponding error is in Table 5-8.

Table 5-5: Bend & Twist Results (BTE Load Case)

	Bending (inches)			*Twist (radians)*		
Load	*CFC*	*FEA*	*Test*	*CFC*	*FEA*	*Test*
50	0.083	0.062	0.066	-0.0022	-0.0080	-0.0083
80	0.132	0.100	0.105	-0.0036	-0.0128	-0.0133
100	0.166	0.124	0.133	-0.0045	-0.0159	-0.0168

Table 5-6: Predicted Bend & Twist Errors (BTE Load Case)

	Bend Error		*Twist Error*	
Load	*CFC*	*FEA*	*CFC*	*FEA*
50	25%	6%	73%	4%
80	26%	5%	73%	4%
100	25%	7%	73%	5%

Table 5-7: Bend & Twist Results (BLE Load Case)

	Bending (inches)			*Twist (radians)*		
Load	*CFC*	*FEA*	*Test*	*CFC*	*FEA*	*Test*
50	0.064	0.048	0.051	-0.0009	0.0056	0.0057
80	0.102	0.077	0.082	-0.0015	0.0089	0.0093
100	0.128	0.100	0.102	-0.0018	0.0113	0.0115

Table 5-8: Predicted Bend & Twist Errors (BLE Load Case)

	Bend Error		*Twist Error*	
Load	*CFC*	*FEA*	*CFC*	*FEA*
50	25%	7%	116%	2%
80	25%	6%	116%	4%
100	25%	2%	116%	2%

At all loads, the bending predicted by the CFC is 25% greater than the actual bending in the specimen. The consistency of this error between the load cases indicates that the CFC can predict the bending trend, however the magnitude is greater. As discussed in Chapter 3, the CFC model contains only cover panels and web panels. The stiffness of the aluminum and composite brackets is not included in the closed form analysis. Therefore the CFC model is not expected to be as stiff as the actual wing box specimen.

The twist prediction is significantly different from the experimental results. The error is 73% when loaded on the BTE corner and 116% when loaded on the BLE corner. In addition to the difference in magnitude, the CFC predicts twist that is opposite in sign when loaded on the BLE corner. To determine if the brackets were causing the difference between the predicted and measure results, a finite element analysis of the wing box was carried out without the brackets.

The FEA results still contradict the CFC in wing twist. Therefore the current form of the CFC is not capable of predicting box twist. The analysis method requires some refinement.

A basic assumption made in Rehfield's tailored box model is that only the extension-shear coupling terms are significant during box bending[6]. In other words the cover panels only undergo extension and not out-of-plane bending. Based on this assumption, the CFC neglects the bend-twist coupling terms in the laminate D matrix when calculating the twist and bending of the wing box. The axial strains listed in Table 5-4 show that near the tip panel bending is significant when compared to extension. Examination of the transverse gages indicates that the panels are nearly in pure bending in the chord-wise direction as shown in Table 5-9. These measurements indicate that the assumption of no significant panel bending is no longer valid at the tip. The bend-twist coupling terms in the laminate D matrix may need to be considered in the calculations.

Table 5-9: Transverse Back-to-Back Strains

	100 lb BTE Load		100 lb BLE Load	
Upper Cover Location	*Top Gage (με)*	*Bottom Gage (με)*	*Top Gage (με)*	*Bottom Gage (με)*
Center Mid-span	-22	53	23	15
Trailing Edge Tip	227	-233	-232	244
Leading Edge Tip	-257	276	285	-262

The transverse bending strains are caused by local bending in the cover panels. With these local deformations the wing box does not maintain a constant cross-section throughout the span, which is another assumption made in the derivation of the CFC. The global box stiffnesses (C_{44}, C_{45}, and C_{55}) are no longer constant and the bending and twist calculations are affected.

The chord-wise bending of the cover panels may partly be a product of the manner in which the load is introduced into the test article. If this is the case, it might be possible to redesign the test such that it better represents the CFC model. However the loading conditions of a real aircraft wing must be considered when evaluating the inadequacies of the CFC model.

Chapter 6 : Concluding Remarks

A 32 in. x 12 in. x 2.27 in. wing box specimen was designed and fabricated to demonstrate elastic tailoring. The wing box consists of two tailored cover panels with 35° and 45° angle plies and two balanced/symmetric web panels. The specimen was loaded as a cantilever beam with two individual tip corner loads to represent a wing structure under span-wise bending and chord-wise twisting. The test load range was 0 to 100 lbs. Displacement and strain data were gathered to characterize the response.

The wing box specimen was analyzed using two separate methods. First a Closed Form Code (CFC) based on a single cell box theory was derived to predict twist and bending of the wing box. Second a Finite Element Analysis (FEA) was used to predict the displacement and strain response of the box specimen. The measured results were compared with the predicted results for analysis validation.

6.1 Conclusions

The finite element analysis adequately predicted both strains and displacements. Trends in box behavior correlated well with the finite element solution. The magnitude of the error in the displacement prediction is generally within 7%. Predictions of average bending and twist are within 4-7%. The results indicate that the finite element analysis would accurately predict the behavior of a full-scale tailored structure. Prediction error should decrease in a larger structure due to reduction of the influence of small inaccuracies in measurements and imperfections.

The CFC model was only partially validated. The magnitude of bending is consistently 25% greater than the measured values from the wing box specimen. This error can partly be attributed to the presence of stiffening structures such as brackets in the specimen that are not included in the CFC model. While further development and testing is required, the box bending prediction of the closed form analysis may be applied successfully to a larger wing box. The CFC proved to be unable to accurately predict the twist of the test specimen. When developing the governing equations for the tailored box model, an assumption is made that bending in the cover panels is insignificant and that extension-shear coupling is the dominant mechanism. Measured strains taken from the test specimen indicate that bending in the cover panels is a significant factor near the wing tips. The cover panels undergo both span-wise and chord-wise bending. This panel bending causes bend-twist coupling within the cover panels, which contradicts the assumptions made in the CFC derivation. Therefore the CFC twist model is not suitable for this test specimen and needs further development before it can be used as a design tool.

6.2 Recommendations for Future Work

While the finite element analysis was able to accurately predict the displacement and strain trends of the wing box specimen, the errors in some areas are high (i.e., >10%). These errors generally occur in areas of the box with small displacements or strains and could be attributable to measurement sensitivities. A next step would be to apply these analysis techniques to a larger or full-scale structure. A larger model would produce smaller percentage errors to due to measurement inaccuracies and imperfections in the wing box.

It was apparent from the response of the wing box specimen that tailored structures can undergo camber deformations. Previous analytical research has been performed regarding chord-wise tailoring, however the analysis method has not been compared to the response of a test specimen. Future wing box specimens can be designed to be chord-wise deformable to validate that aspect of aeroelastic tailoring.

The adhesive layer between the brackets and the panels failed due to a combination of shear and peeling. A second specimen may benefit from the addition of fixtures to prevent peeling forces on the adhesive.

The CFC requires further development and revisions before it can be validated. However when the code is ready, it has the potential to be much more flexible in terms of geometry of the model. The code can be expanded to allow for a wing taper (i.e., variable cross-section), sweep, stiffeners, and other features. Allowing multiple material properties and load cases would also be necessary.

The ultimate goal in aeronautical engineering is always to achieve the desired performance at the minimum weight. It would be useful to put a validated CFC in the form of a constrained optimization program. This could potentially allow an engineer to specify bending, twist, and camber requirements and search for a minimum weight solution in the range of feasible designs.

References

1. Patil, M.J., "Aeroelastic tailoring of composite box beams," *AIAA Meeting Papers on Disc* [CD-ROM], Reno, NV, 1997.

2. Sherrer, M.H., Hertz, T.J., and Shirk, M.H., "A Wind Tunnel Demonstration of the Principle of Aeroelastic Tailoring Applied to Forward Swept Wings," *Journal of Aircraft, 1981 pp. 976-983.*

3. Roger, W.A., Braymen, W.W., Shirk, M.H., "Design, Analyses, and Model Tests of an Aeroelastically Tailored Lifting Sufrace," *AIAA Aircraft Systems and Technology Conference*, Dayton, OH, August 11-13, 1981, AIAA-81-1673.

4. Valisetty, R.R. and Rehfield, L.W., "Simple Theoretical Models for Composite Rotor Blades," Georgia Institute of Technology, Atlanta, GA, 1984.

5. Hodges, R.V., Nixon, M.W., and Rehfield, L.W., "Comparison of Composite Rotor Blade Models: A Coupled-Beam Analysis and an MSC/NASTRAN Finite-Element Model," NASA Technical Memorandum 89024, March 1987

6. Rehfield, Lawrence W. "A Refined Simple Model for Tailoring Box Beams with Composites," *42nd AIAA/ASME/ASCE/AHS/ASC Structures, Structural Dynamics, and Materials Conference*, Seattle, WA, April 16-19, 2001, AIAA 2000-1333, published on CD-ROM, AIAA, Reston, VA, 2001.

7. Cheung, R. H.,"Some Basic Strategies for Aeroelastic Tailoring of Wings with Bend-Twist Coupling," MS Thesis, University of California, Davis, 2002.

8. Jones, R.M., *Mechanics of Composite Materials,* 2nd ed., Taylor & Francis, Inc., Philadelphia, 1999, Chaps. 2, 4.

9. Grimsley, B. W., Song, X., Hubert, P., Cano, R. J., Loos, A. C., and Jensen, Modeling of the Vacuum Assisted Resin Transfer Molding Process: Permeability and Compaction Characterization, ASC Conference, Gainesville, FL, October 2003.

10. "Standard Test Method for Tensile Properties of Polymer Matrix Composite Materials," ASTM D 3039/D 3039M – 00, West Conshohocken, PA, 2000.

11. Patran, Ver. 2003, MSC. Software Corporation, Santa Ana, CA, 2003.

12. Ranking, C.C, Brogan, F. A., and Loden, W.A, "STAS User Manual," Version 4.0, Lockheed Martin Missiles & Space Co., Inc, Palo Alto, CA, 2001.

13. Magnamite IM7 (5000) Product Data Sheet, Hexcel Corporation, March 2000.

14. VR56-19 Aircraft Structural VARTM Resin Data Sheet, Applied Poleramic Inc., Banicia, CA, 2000.

15. Hysol EA 934NA Data Sheet, Loctite Aerospace, Bay Point, CA, 2000.

Appendix: Closed Form Code

The script listed here is code for the closed form analysis. This code is written for Matlab v6. The values in the input section can be modified to represent a wing box specimen with tailored cover panels (up to 2 angle plies) and web panels.

Main Program

```
%=========================================================================
% COMPOSITE WING BOX ANALAYSIS TOOL
% Author: Dulnath Wijayratne
%
% Description: The purpose of this program is to provide an analysis tool for the early design
%stages aeroelastically tailored wings. Specifcally, this program outputs the twist and bending
%as a function of span for a structural composite wing box given geometric, material, and
%loading parameters.
%
%   Wing Diagram
%
%        ^ y
%        |
%        |
%        |                    Leading Edge
%        |_____________________________________________________________
%        |                                                             | TIP
%        |                                                             |
%    ROOT ----------------> x          TOP VIEW OF WING BOX             |
%        |                                                             |
%        |_____________________________________________________________|
%
%                            Trailing Edge
%
%
% Notes: -Boundary Conditions assume wing root is fixed.
%            -This program limits load to tip edge.
%             -Maximum of 2 angle plies
%
%=========================================================================
```

```
clear
clc



%#########################################################################
% USER INPUT!
%#########################################################################

%Geometric Data (inches)
%**********************

C=12;    %Structural box chord (width)
H=2.27;     %Box Height
L=31.6;    %Box Length (span)

%Material Data
%*************

%Material Name: IM7 Fiber in VR56-19 VARTM Resin
E11=20100000;
E22=1470000;
G12=640000;
v12=.31;

%Top Cover Panel
u_thick=.086;     %Panel thickness (inches)
u_ply=14;         %# of plies
u_theta1=35;      %Specify Angle Ply 1
u_theta2=45;      %Specify Angle Ply 2
u_sequence=[35;90;35;45;90;45;90;90;45;90;45;35;90;35];  %stacking sequence

%Lower Cover Panel
l_thick=.086;     %Panel thickness (inches)
l_ply=14;         %# of plies
l_theta1=-35;      %Specify Angle Ply 1
l_theta2=-45;      %Specify Angle Ply 2
l_sequence=[-35;90;-35;-45;90;-45;90;90;-45;90;-45;-35;90;-35];  %stacking sequence

%Front (leading edge) web panel
f_thick=.05;     %Panel thickness (inches)
f_ply=4;         %# of plies
```

```
f_theta1=45;      %Specify Angle Ply 1
f_theta2=-45;     %Specify Angle Ply 2
f_sequence=[45;-45;-45;45];  %stacking sequence

%Rear (trailing edge) web panel
r_thick=.05;     %Panel thickness (inches)
r_ply=4;         %# of plies
r_theta1=45;      %Specify Angle Ply 1
r_theta2=-45;     %Specify Angle Ply 2
r_sequence=[45;-45;-45;45];   %stacking sequence


%Load Data
%**********

P=100;  %Load (lb)
y=-6;      %Offset from x-axis (inches)     Note: Load must be on tip edge


%Program Data
%***********
e=100;      %Number points generated over the span
%#########################################################################


%=========================================================================
%Calculations

%Ply thicknesses
u_h=u_thick/u_ply;
l_h=l_thick/l_ply;
f_h=f_thick/f_ply;
r_h=r_thick/r_ply;

%Reduced Stiffness Matrix
Q0 = Qmatrix(E11,E22,G12,v12);

%Transformed Stiffness Matrices
Q90 = QTransform(Q0,90);

u_Qtheta1 = QTransform(Q0,u_theta1);
u_Qtheta2 = QTransform(Q0,u_theta2);
```

```
l_Qtheta1 = QTransform(Q0,l_theta1);
l_Qtheta2 = QTransform(Q0,l_theta2);

f_Qtheta1 = QTransform(Q0,f_theta1);
f_Qtheta2 = QTransform(Q0,f_theta2);

r_Qtheta1 = QTransform(Q0,r_theta1);
r_Qtheta2 = QTransform(Q0,r_theta2);



% A,B, and D Matrices
[Au] = abd(u_sequence,u_h,u_theta1,u_theta2,Q0,u_Qtheta1,u_Qtheta2,Q90);

[Al] = abd(l_sequence,l_h,l_theta1,l_theta2,Q0,l_Qtheta1,l_Qtheta2,Q90);

[Af] = abd(f_sequence,f_h,f_theta1,f_theta2,Q0,f_Qtheta1,f_Qtheta2,Q90);

[Ar] = abd(r_sequence,r_h,f_theta1,f_theta2,Q0,r_Qtheta1,r_Qtheta2,Q90);


%Wall Plane Stress Stiffnesses
K11u = Au(1,1)-(Au(1,2))^2/Au(2,2);          %Upper Extensional
K12u = Au(1,3)-(Au(1,2)*Au(2,3))/Au(2,2);    %Upper Coupling
K22u = Au(3,3)-(Au(2,3))^2/Au(2,2);          %Upper Shear

K11l = Al(1,1)-(Al(1,2))^2/Al(2,2);          %Lower Extensional
K12l = Al(1,3)-(Al(1,2)*Al(2,3))/Al(2,2);    %Lower Coupling
K22l = Al(3,3)-(Al(2,3))^2/Al(2,2);          %Lower Shear

K11f = Af(1,1)-(Af(1,2))^2/Af(2,2);          %Front Extensional
K12f = Af(1,3)-(Af(1,2)*Af(2,3))/Af(2,2);    %Front Coupling
K22f = Af(3,3)-(Af(2,3))^2/Af(2,2);          %Front Shear

K11r = Ar(1,1)-(Ar(1,2))^2/Ar(2,2);          %Right Extensional
K12r = Ar(1,3)-(Ar(1,2)*Ar(2,3))/Ar(2,2);    %Right Coupling
K22r = Ar(3,3)-(Ar(2,3))^2/Ar(2,2);          %Right Shear


%Global "Box" Stiffnesses
C44 = ((C*H)^2/(C+H)^2) * ((K22u+K22l)*C + (K22r + K22f)*H);
C45 = ((C*H)^2/(2*(C+H))) * (K12l-K12u);
C55 = ((C*H^2)/4) * (K11u+K11l);
```

```
Betasq=(C45^2)/(C44*C55);

%Deformation Parameters
i=L/e;
j=0;

for m=0:i:L
   j=j+1;
   prate = (P/(C44*C55*(1-Betasq))) * (C55*y-C45*(m-L));
   p = (P/(C44*C55*(1-Betasq))) * ((C55*y+C45*L)*m-(C45*m^2)/2);

   bendrate = (P/(C44*C55*(1-Betasq))) * (C45*y-C44*(m-L));
   bend = (P/(C44*C55*(1-Betasq))) * ((C45*y+C44*L)*(m^2/2)-(C44*m^3/6));

   x(j)=m;

   phi_rate(j)=prate;
   phi(j)=p;

   z_rate(j)=bendrate;
   z(j)=bend;
end

[UTEC,ULEC] = graphics(x,phi,z,phi_rate,z_rate,e,C,H,L)

bend=z(101)
twist=phi(101)
```

Q Matrix Subroutine

```
%--------------------------------------------------------------------------
% This function will return the Q (reduced stiffness) matrix
%
% Input: E11,E22,G12,v12
% Output: Q
%--------------------------------------------------------------------------

function Q = Qmatrix(E11,E22,G12,v12)

v21=v12*(E22/E11);
Q11=E11/(1-v12*v21);
Q22=E22/(1-v12*v21);
Q12=(v12*E22)/(1-v12*v21);
```

```
Q66=G12;
Q=[Q11 Q12 0; Q12 Q22 0; 0 0 Q66];
```

Q Transformation Subroutine

```
%-------------------------------------------------------------------------------------------------------------
% This program will return the Q (reduced stiffness) matrix and two Qbar (transformed reduced
stiffness) matrices.
% The user must enter principle material (ply) properties and two angles (for Q transformation).
%-------------------------------------------------------------------------------------------------------------

clear
clc

E11=20100000;
E22=1470000;
G12=640000;
v12=.31;

d1=45;
d2=90;

v21=v12*(E22/E11);
Q11=E11/(1-v12*v21);
Q22=E22/(1-v12*v21);
Q12=(v12*E22)/(1-v12*v21);
Q66=G12;
Q=[Q11 Q12 0; Q12 Q22 0; 0 0 Q66]

R=[1 0 0; 0 1 0; 0 0 2];
Rinv=inv(R);

%***Qbar for first angle***
theta1=d1*(3.14159/180);

T11=(cos(theta1))^2;
T12=(sin(theta1))^2;
T13=2*sin(theta1)*cos(theta1);
T21=(sin(theta1))^2;
T22=(cos(theta1))^2;
T23=-2*sin(theta1)*cos(theta1);
```

```
T31=-sin(theta1)*cos(theta1);
T32=sin(theta1)*cos(theta1);
T33=(cos(theta1))^2-(sin(theta1))^2;
T1=[T11 T12 T13; T21 T22 T23; T31 T32 T33];

T1inv=inv(T1);
Qbar1=T1inv*Q*R*T1*Rinv

%***Qbar for second angle***
theta2=d2*(3.14159/180);

T11=(cos(theta2))^2;
T12=(sin(theta2))^2;
T13=2*sin(theta2)*cos(theta2);
T21=(sin(theta2))^2;
T22=(cos(theta2))^2;
T23=-2*sin(theta2)*cos(theta2);
T31=-sin(theta2)*cos(theta2);
T32=sin(theta2)*cos(theta2);
T33=(cos(theta2))^2-(sin(theta2))^2;
T2=[T11 T12 T13; T21 T22 T23; T31 T32 T33];

T2inv=inv(T2);
Qbar2=T2inv*Q*R*T2*Rinv
```

A Matrix Subroutine

```
%Calculates the A matrix of a laminate with plies of 0, 90, and up to
%two intermediate angles (theta 1 and theta 2).

function [A] = abd(sequence,t,theta1,theta2,Q0,Q1,Q2,Q90)

%Initialize
A=zeros(3,3);
M=zeros(3,3);
n=length(sequence);
ply=n;

for s=1:n

  %Establishing layer Q matrix
  if sequence(s,1)==0
    M=Q0;
  elseif sequence(s,1)==theta1
```

```
    M=Q1;
  elseif sequence(s,1)==theta2
    M=Q2;
  elseif sequence(s,1)==90
    M=Q90;
  end

      %Calculating A
      for i=1:3
         for j=1:3
            A(i,j)=A(i,j)+M(i,j)*t;
         end
      end
  ply=ply-1;
end
```

REPORT DOCUMENTATION PAGE

Form Approved
OMB No. 0704-0188

1. REPORT DATE *(DD-MM-YYYY)*	2. REPORT TYPE	3. DATES COVERED *(From - To)*
01- 12 - 2004	Contractor Report	

4. TITLE AND SUBTITLE

Validation of Design and Analysis Techniques of Tailored Composite Structures

5a. CONTRACT NUMBER

5b. GRANT NUMBER

5c. PROGRAM ELEMENT NUMBER

6. AUTHOR(S)

Wijayratne, Dulnath D.

5d. PROJECT NUMBER

NCC1-03008

5e. TASK NUMBER

5f. WORK UNIT NUMBER

23-762-55-TA

7. PERFORMING ORGANIZATION NAME(S) AND ADDRESS(ES)

The George Washington University
Joint Institute for Advancement of Flight Sciences
Langley Research Center
Hampton, VA 23681

8. PERFORMING ORGANIZATION REPORT NUMBER

9. SPONSORING/MONITORING AGENCY NAME(S) AND ADDRESS(ES)

National Aeronautics and Space Administration
Washington, DC 20546-0001

10. SPONSOR/MONITOR'S ACRONYM(S)

NASA

11. SPONSOR/MONITOR'S REPORT NUMBER(S)

NASA/CR-2004-212650

12. DISTRIBUTION/AVAILABILITY STATEMENT

Unclassified - Unlimited
Subject Category 39
Availability: NASA CASI (301) 621-0390

13. SUPPLEMENTARY NOTES

Thesis to the Faculty of Structures and Dynamics Department, The George Washington University, in partial fulfillment of the requirements for the Degree of Master of Science, August 2004. Langley Technical Monitor: Dawn C. Jegley.
An electronic version can be found at http://techreports.larc.nasa.gov/ltrs/ or http://ntrs.nasa.gov

14. ABSTRACT

Aeroelasticity is the relationship between the elasticity of an aircraft structure and its aerodynamics. This relationship can cause instabilities such as flutter in a wing but it is possible to use aeroelastic tailoring to cause an aircraft structure to respond favorably to flight loading conditions. This research investigates the ability to design and analyze tailored structures made from filamentary composites. A validation experiment has been performed on a small-scale filamentary composite wing box. The box is tailored such that its cover panels induce a global bend-twist coupling under an applied load. A closed form analysis based on a theoretical model of a single cell tailored box beam and a finite element analysis are used to analyze the structures. The comparison of predicted and experimental results show that the finite element analysis is capable of predicting displacements and strains to within 10% and the closed form code is able to predict the wing box bending to25% of the measured value but resulted in larger errors in the twist prediction. Initial assumptions in the closed form code limit its accuracy.

15. SUBJECT TERMS

Structural tailoring; Aeroelastic; VARTM; Composite; Graphite-epoxy

16. SECURITY CLASSIFICATION OF:			17. LIMITATION OF ABSTRACT	18. NUMBER OF PAGES	19a. NAME OF RESPONSIBLE PERSON
a. REPORT	b. ABSTRACT	c. THIS PAGE			STI Help Desk (email: help@sti.nasa.gov)
					19b. TELEPHONE NUMBER *(Include area code)*
U	U	U	UU	85	(301) 621-0390